A New Horizon of Accelerator Physics

Shun-ichi HASEGAWA, Hirotada NANJO,* Takeshi OGATA,**
Michinori SAKATA,*** Kojiro TANAKA* and Nobuo YAJIMA****

Science and Engineering Research Laboratory, Waseda University
Tokyo
**Department of Physics, School of Science and Engineering*
Waseda University, Tokyo
***Faculty of Science, Kwansei Gakuin University, Nishinomiya*
****Department of Physics, Konan University, Kobe*
*****Research Institute for Fundamental Physics, Kyoto University*
Kyoto

(Received April 27, 1970)

Introduction

In the spring of 1965, our group started to study the multiple meson production in the accelerator energy regions on the basis of our understanding on high energy nuclear interactions so far made clear through our cosmic-ray research work in Japan. It was the time when the cosmic-ray experiment confirmed that the multiple meson production takes place through an intermediate state—called a fire-ball.[1)~3)]

We focussed our particular attention on the H-quantum hypothesis[4)] proposed by one of us (S. H.) among the proposed theories or models of multiple meson production. The H-quantum hypothesis insists that there exists an elementary "unit" in the fire-ball and it works as energy quantum in the multiple meson production. The mass of H-quantum was estimated as two to three times of the nucleon rest energy—the same order of magnitude of mass of baryon and anti-baryon system—through the study of the angular distribution of high energy cosmic-ray jets in the nuclear emulsions observed by various laboratories in the world at that time.[5)] The analysis of nuclear interactions observed by emulsion chamber experiments on Mt. Norikura and Mt. Chacaltaya was also consistently understood on the basis of the H-quantum hypothesis.

Yokoi and one of us (S. H.)[6)] derived a formula to estimate the four-mometum transfer between two groups of secondary mesons from the angular distribution of jet showers. Results of the analysis with this formula gave a general law for mechanism of production of the H-quantum such that the four-momentum transfer between H-quanta and between a nucleon and a H-quantum is about the same magnitude with H-quantum mass, and it was called a law of constant four-momentum transfer or constant virtuality.

Considering these characteristics above described together with the experimental facts that jet phenomena occur with the geometrical cross section, it was concluded that the H-quantum is closely connected with the inner structure of mesons as was suggested by the composite model of elementary particles proposed by Sakata[7] in 1955.

A number of heavy mesons—resonances—have been found by the accelerator experiments after the proposal of H-quantum hypothesis. Different natures found between H-quantum and heavy mesons have presented us with a fundamental question, as suggested by Taketani,[8] how the upper limit of the mass of heavy mesons is.

Now, it is of deep significance to study the H-quantum production just above the threshold energy. One expects that it should be observable in the accelerator energies of present time when one compares the available energy in C. M. S. with the mass of H-quantum. But, up to that time, at the beginning of 1966, the main attention of the study of elementary particles by the accelerators had been concentrated on exact measurement of cross section of elastic scattering, production of a number of resonance states of baryon and meson and so on. Multiple meson production had never been the central problem and the statistics of published data had never been enough.

One could summarize the qualitative nature of multiple meson production which had been made clear up to that time by the accelerator experiments as follows:

It was established that the production of a single or double mesons in energy region up to several GeV takes place mainly through the isobaric states of nucleon, showing strong forward and backward collimation in the angular distribution of secondary mesons in C. M. S. and small four-momentum transfer.[9] One may expect that this character remains as the energy is going higher. But there may occur some complicated situation such as double isobaric production, heavy boson production and so on.

Meanwhile, the angular distribution of secondary mesons in high multiplicity events seems to be almost isotropic in C. M. S. It was difficult to understand for these events how the multiple meson production does take place.

Hence, one may naturally raise the hypothesis that H-quantum production is going to be the main channel when the available energy exceeds the threshold of production. This hypothesis seemed to be supported by the following facts.

The distribution of the transverse momentum of secondary mesons observed in accelerator energies is quite similar to the one in the cosmic-ray energies. Multiplicity distribution of secondary meson observed in bubble chamber film is also similar to the one of H-quantum decay analyzed in the cosmic-ray jet data.

At first, we were able to get two emulsion stacks exposed to 22.6 and 24 GeV/c proton beam at CERN and started to measure the angular distribution of secondary mesons. The systematic analysis of the forward and backward asymmetry in C. M. S. observed in the angular distribution of secondary mesons of individual event was taken as the first main subject. More than three hundred interactions were found in the emulsion stacks by the track following scanning which could be identified as the collision of a proton with a proton or with a quasi-free nucleon in the nuclear emulsions. After grouping the jets by magnitude of the asymmetry, one could find the existence of the regularity which could be understood that mesons are emitted isotropically from the emitting center moving with the definite velocity forward or backward in the C. M. S., $\gamma_H^* \approx 1.3$. It was also striking that the regularity above mentioned is independent of the multiplicity of the events for $n_s \geq 4$. The knowledge on average values of the transverse momentum and the multiplicity of secondary mesons given mass of emitting center as twice to thrice of the nucleon rest energy. These results are just what the H-quantum hypothsis insisted.

As mentioned often, however, in the text, it is quite difficult to identify kinds of the individual particles, to measure their energy and to be free from complexity of contamination that the interaction occurs with heavy target nuclei in the nuclear emulsion.

It is natural that we desired to proceed to the analysis of the hydrogen bubble chamber films as our next step in order to confirm our results obtained in the nuclear emulsion analysis avoiding the difficulty above mentioned. Fortunately, we could get 1000 pictures of 10 GeV/c π^--beam in CBH 81 by kind arrangement of Prof. Leprince-Ringuet and Prof. C. M. G. Lattes and Prof. Y. Fujimoto. This is quite fortunate for us in the following two points. We have the question for a long time whether the multiple meson production by the meson has the same character as that of nucleon or not. Furthermore, one can solve the question which of the H-quantum and a hypothetical excited baryon production is of essential process in the high energy collisions.

It was the first time for us to analyze the bubble chamber films, so all the program should be started from the beginning. The time lag is quite long. Waseda group, however, completed the analysis with one projector and a computer OKITAC 5090H. The multiple meson production of higher multiplicity ($n_s = 6, 8$) is studied at first, because the characteristics of the fire-ball production should be clearest in the events of this category.

The results are summarized as follows. The production of a fire-ball is established by balance of momentum of the secondary particles. The mechanism of collision, therefore, is found to be composed of the three-body reaction, that is, a survived pion (leading pion), a recoil nucleon and a created fire-ball. The created fire-ball moves forward or backward with Lorentz factor $\gamma_H^* \approx 1.1$ in C. M. S. Mass of the fire-ball is obtained as 2.4 ± 0.4 GeV. The standard

deviation of the mass distribution is obtained as about 600 MeV.

Four-momentum transfer of leading pion Δ_π and of recoil proton Δ_p are measured, respectively. Both the average values are $\sqrt{-\Delta^2} \approx 1$ GeV/c. These are quite consistent with the one of cosmic-ray jets obtained by Yokoi and Hasegawa method.

Just in 1968, an enormous amount of data were published for the analysis of multiple meson production by the incident proton and meson of various energies in the foreign laboratories. It includes angular distribution of secondary particles, correlation of momentum of longitudinal and transverse components, invariant mass of a group of secondary mesons, and so on. In part III of the text, we shall discuss the experimental evidence of H-quantum production summarizing all the data which are in our hand.

Part I. Emulsion experiment*)

In this part, we shall discuss the experimental results obtained by our measurement of interaction of 22.6 and 24 GeV/c proton with free or quasi-free nucleon in the nucleus in the nuclear emulsion. The experimental procedure and the results such as mean free path, prong number distribution and so on have already been published in a short note.[10]

Therefore, we present here only a brief summary of our experimental results which were fully described in Refs. 10) and 11), and let us concentrate the discussion on the analysis of the angular distribution of secondary mesons and its physical meaning along the line of thought described in the previous sections.

§1. Brief summary of the results

1–1) *Experimental procedure*

In this experiment, we used two kinds of stacks of Ilford G–5 pellicles, each 12 cm × 20 cm × 600 μm, exposed to the 22.6 and 24 GeV/c external proton beam of the CERN proton synchrotron. The proton beam entered the stacks along the direction nearly parallel to the plane of the emulsion. The average flux value was found about 6×10^4 particles per cm^2. The beam tracks were scanned and followed until they interacted in the emulsion or left the plate. The scanning was made inside of a margin of 1 cm from the edge to minimize the distortion effect. The magnification used for scanning was ×60 objectives ×10 eyepieces and ×1.25 optical length. After checking the scanning, it was found that the nuclear interactions were detected without any serious bias except the extremely small angle scattering.

*) By Shun-ichi Hasegawa, Hirotada Nanjo, Takeshi Ogata, Michinori Sakata, Kojiro Tanaka and Nobuo Yajima.

1-2) *General results*

A total track length of 620.4 m has been followed to observe 1656 interactions of all types. A summary of the results is presented in Table I.*)

Table I. A summary of the results.

Laboratory	Primary momentum (GeV/c)	Track length followed (m)	No. of interaction found	Mean free path (cm)	Mean multiplicity
K. G.	22.6	220.80	594	37.2±1.5	5.6±0.3
Nagoya	24	200.09	547	36.6±1.6	5.4±0.3
Waseda	24	199.50	515	38.8±1.7	5.8±0.3
Total	—	620.39	1656	—	—

Laboratory	No. of interactions with $N_h \leq 1$, $n_s \geq 3$	Mean free path (cm) for $N_h \leq 1$, $n_s \geq 3$	% of interactions with $N_h \leq 1$	Mean multiplicity for $N_h \leq 1$, $n_s \geq 3$
K. G.	122	182±16	21	4.4±0.4
Nagoya	101	200±20	19	4.0±0.4
Waseda	98	205±21	19	4.1±0.4
Total	321	—	—	—

1-2-a) *Mean free path*

In this experiment, the mean free path for the inelastic collisions of 22.6 and 24 GeV/c proton with emulsion nuclei is found to be 37.2±1.5 cm and 37.6±1.2 cm, respectively, which are consistent with the results obtained by other authors[12)~14)] (see Fig. 1). As can be seen from Fig. 1, the interaction mean free path in the nuclear emulsion of a high energy proton remains nearly constant, of 40cm, up to the cosmic-ray energy region. The observed mean free path has no significant differences from the geometrical collision mean free path

$$\lambda_{\text{geom}} = 1/\sum_i N_i \pi (r_0 \cdot A_i^{1/3})^2, \tag{1}$$

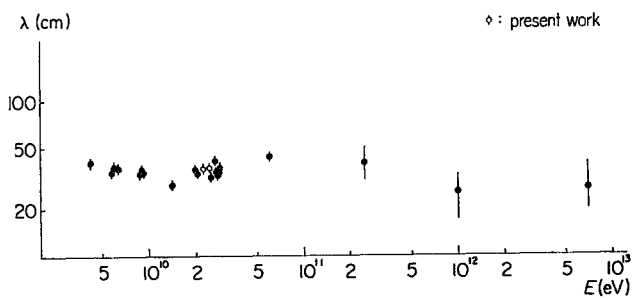

Fig. 1. Collision mean free path of proton in emulsion as a function of primary energy.

*) Afterwards, we collected more 65 events of n_s=7, 8, 9 and 10 by track following scanning in order to analyze the angular distribution in a better statistics for higher multiplicity phenomena.

where A_i and N_i are the mass number and the number density of i-nucleus in emulsion, respectively, and r_0 is a constant of dimension of length with order of magnitude of the pion Compton wave length. From Eq. (1) the geometrical mean free path is 36.6cm, when r_0 is taken to be 1.2×10^{-13}cm.

The mean free path for events of $N_h=0,1$ (N_h is the total number of the "grey" and "black" tracks in a star) is found to be 182 ± 16 cm for 22.6 GeV/c and 202 ± 15 cm for 24 GeV/c, respectively. The events with $n_s\leq2$ are not taken into account in obtaining this value. The observed values are much smaller than expected collision mean free path for proton-hydrogen interaction in the nuclear emulsion, $\lambda_{exp}=487$cm, estimated from a value of hydrogen content in the emulsion, 3.34×10^{22} atoms/cm^3.[13] This implies that at least about 60 percent of the observed events with $N_h=0,1$ should be assigned to the interactions of a proton with a bound-nucleon.

1-2-b) *Prong number distribution*

The observed statistics for correlation of N_h vs n_s are summarized in Table II, where N_h and n_s are the number of heavily ionized tracks and of thin tracks, respectively. In our experiment the thin track is defined as it has ionization lower than 1.4 times of minimum ionization.

Figure 2 shows the dependence of the average multiplicity on primary energy found by various authors.[14),15),26),33)] We must notice here that the multiplicity of the individual event considerably fluctuates at a given primary

Table II. Correlation between n_s and N_h.

n_s	0	1	2	3	4	5	6	7	8	9	10	11	12	13	14	15	16	17	18	19	20	21	22	23	≥24
18																							1		1
17												1						1		1			1		
16					1	1		2				1					1						1		
15									1				1	1		2			1	1	1				
14		1							1					2			1			1					1
13	1	1			1	2		1			2	1				4		1		1		1	1		3
12	1	1	3	1	2	3		1	3	2	2		2	2	3	1	1	2	5	2	2	1			2
11		2		2		3	3	1	1	1	2	3	3	4	1	6	4			2			1	1	4
10	2	2	4	2			3		6	3	2	1	4	2	2		2	5	2		1	4		2	4
9	7	7	5	7	2	9	3	9	3	4	3	7	2	8	6	6	3	2	2	1	3	1		2	4
8	9	8	3	8	12	8	4	7	3	8	4	3	1	7	2	4	3		5	2				1	3
7	17	10	6	5	12	9	14	4	6	6	5	11	1	3	4	1	8	2	2	2		1	1	1	2
6	21	16	22	25	16	16	14	12	6	9	11	2	1	6	1		1	3	2			1		1	5
5	23	18	15	21	14	22	16	10	10	2	5	12	6	5	5	2	5		1		2		1	1	1
4	37	34	17	14	20	19	9	9	6	7	3	6	4	7	11	2	4	1		5	5	1		1	1
3	58	45	19	20	13	9	15	3	3	4	3	2		6			2	2	3						2
2	70	17	14	9	12	10	16	7		5		3		2		2		2			1			1	4
1	22	35	7	11	16	12	4	4	6		2	1	1	1		3	2	1		1		1	1		
0			1	1		1	1				1	1													

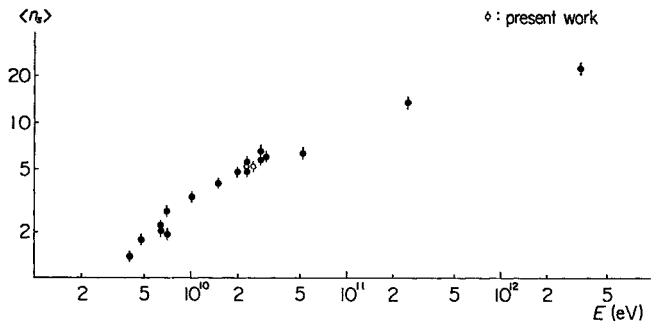

Fig. 2. Mean multiplicity as a function of primary energy.

energy. An increase of mean multiplicity with primary energy at the accelerator energy region is much steeper than at cosmic-ray energy region.

Figures 3 (a) to (e) illustrate distribution of the multiplicity n_s classifying the events by the number of heavy prongs N_h. As can be seen from Fig. 3, a proportion of the events of $n_s=3$ is fairly larger for $N_h=0$ than in the cases of $N_h\geq 1$, hence the average multiplicity for events with $N_h=0$ is smaller than that for the events with other N_h. We have to keep in mind that a large proportion of the events of $n_s=3$ for $N_h=0$ may not be ascribed to the nuclear interaction, but to an effect of contamination of electron which produces a trident in the stacks and of the electron pair created by a proton in the Coulomb field of nucleus.

We can observe a different character in multiplicity distribution between $N_h=0, 1$ events and others. Figures 3(a) and 3(b) show similar distribution, while Figs. 3(c), (d) and (e) show apparently broader spectra and their peaks shift towards larger multiplicities. This indicates that most of the events with $N_h=0$, 1 may be attributed to the collision between a proton and a free or

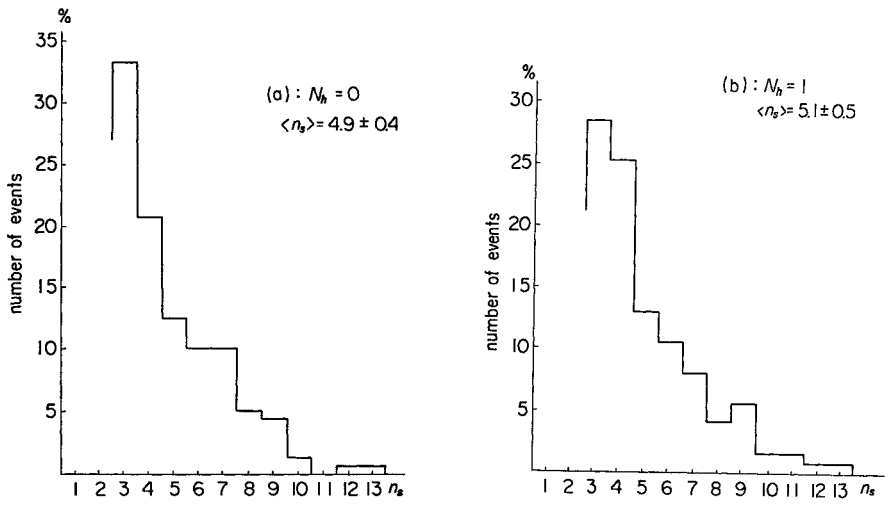

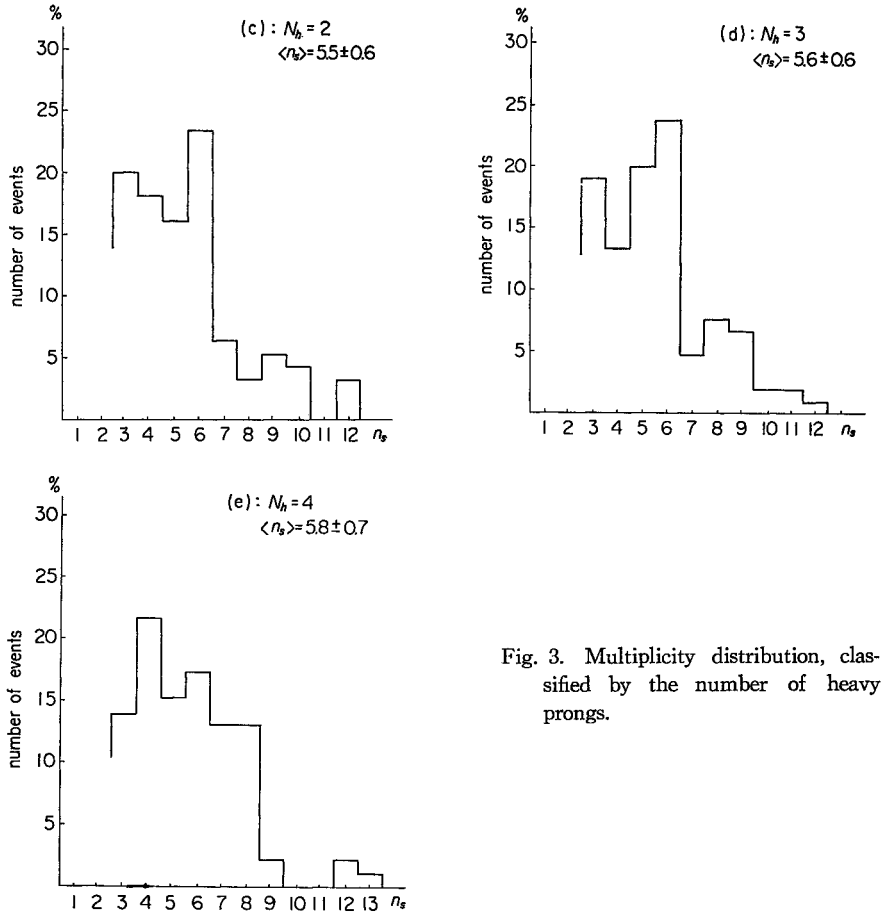

Fig. 3. Multiplicity distribution, classified by the number of heavy prongs.

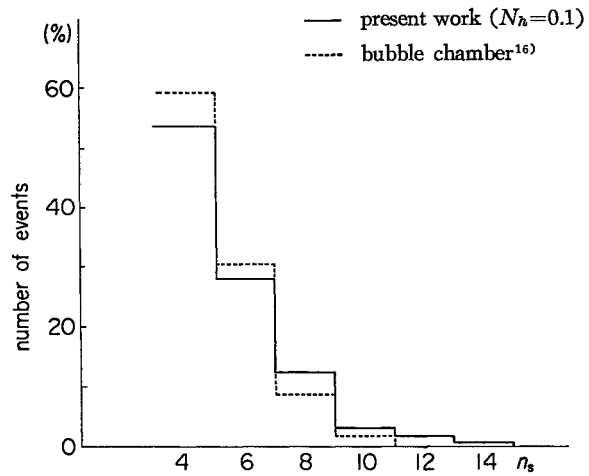

Fig. 4. Comparison of multiplicity distribution for events with N_h=0, 1 with that of hydrogen bubble chamber experiment.

quasi-free nucleon, but the events with $N_h \geq 2$ are strongly affected by secondary collisions in a residual nucleus. Comparing our results with those obtained by hydrogen bubble chamber[16] in Fig. 4, we find their agreement and are not able to find out any effect of residual nucleus in the event of $N_h = 0, 1$. The effect can be detected only through a detailed comparison on a basis of the angular distribution of secondary particles, which will be made in §4.

1-2-c) *Selection of events*

The purpose of our investigation is a study of multiple meson production by nucleon-nucleon interactions. For this purpose, we limit ourselves only in events of $N_h = 0, 1$. This criterion may not be enough to eliminate all effects due to residual nucleus which is mentioned in the previous section. In order to exclude the events associated with secondary interactions in the residual nucleus, the criterion that the inelasticity in the mirror system, K_M should be smaller than 1.4 is applied in this paper. The distribution of K_M for each multiplicities is illustrated in Fig. 5. The K_M is calculated from the formula[17]

$$K_M = (3\langle P_T \rangle / 2M) \sum_{i=1}^{n_s} \tan(\theta_i/2), \tag{2}$$

where M is rest mass of a proton and $\langle P_T \rangle$ the mean value of the transverse momentum of a pion. A fraction of the events rejected by the criterion, $K_M \leq 1.4$, is 0% for $n_s \geq 6$, 12.5% for $n_s = 8$ and 33% for $n_s \geq 9$. Galstyan et al.[18] measured by the pulse magnetic field method the recoil momentum of a proton in the interaction of a proton of 24 GeV/c with emulsion nucleus and obtained the target mass distribution for the event of $N_h \leq 3$ and $N_g \leq 1$, where N_g is the number of grey tracks. According to them, 10% o fthe events for $n_s = 4, 5, 6$ is found in $K_M > 1.5$ and 59% of the events for $n_s \geq 7$ in $K_M > 1.5$. Though the adopted method is different from ours, there is no significant difference in a tendency of the increase of frequency of secondary interaction with multiplicities.

For the analysis on the angular distribution described in the next section, used are the events satisfying the following criteria:

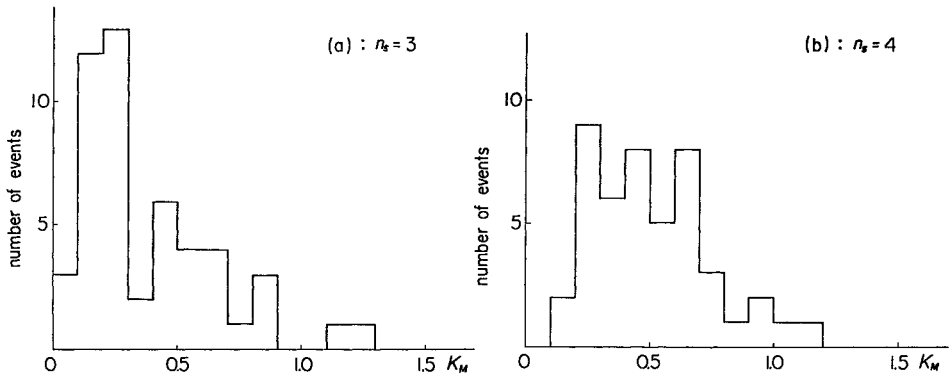

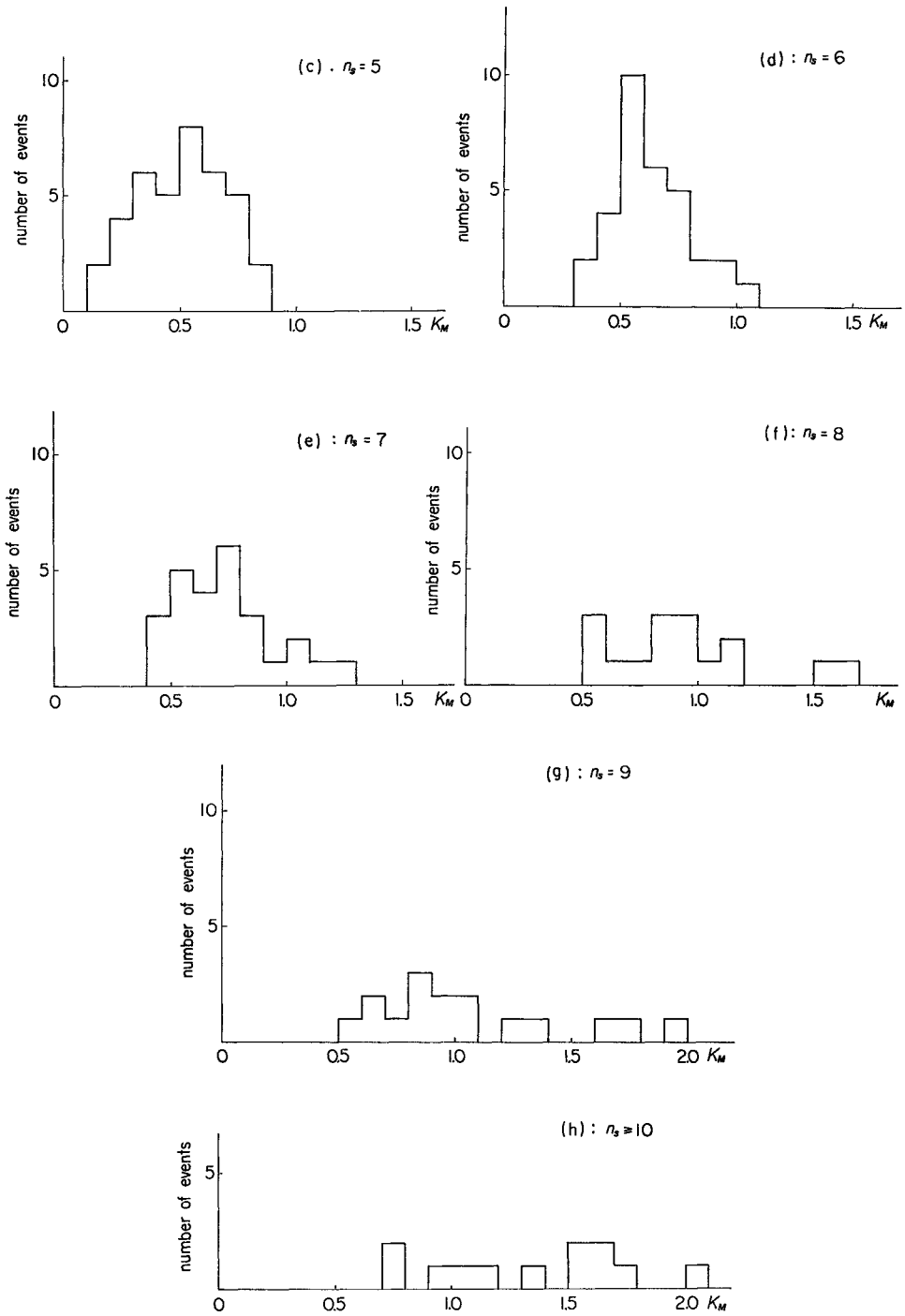

Fig. 5. Distribution of inelasticity in the mirror system, K_M, for events with different n_s.

1) The number of grey or heavy tracks: $N_h \leq 1$.
2) The inelasticity in the Mirror System: $K_M \leq 1.4$.
3) $n_s \geq 4$.

Two hundred and nine events are thus selected among 1656 nuclear interactions.

§2. Angular distribution

2-1) *Angular distribution* (1)

The histogram in Fig. 6 is the composite differential angular distribution in the scale of log $\tan\theta$ for each multiplicity.*) They are compared with a theoretical curve which is calculated by assuming the isotropic distribution in the center of mass system (C. M. S.) and using the momentum distribution obtained by the experiment of hydrogen bubble chamber.[16]

There is seen in Fig. 6 a general tendency that the anisotropy increases with decreasing multiplicity. For the smaller multiplicity events, it is observed that the secondary particles are emitted more frequently in the forward direction in the C. M. S. While, for the large multiplicity events, the angular distribution is found to be nearly isotropic in the C. M. S., having no characteristic of the strong forward excess such as is observed in the smaller multiplicity events. It is not in contradiction with the experimental results by hydrogen bubble chamber.[16] This general tendency seen in the angular distribution may be qualitatively explained as follows: As is discussed in §1-2-a), let us consider a case where the primary proton collides to a bound nucleon

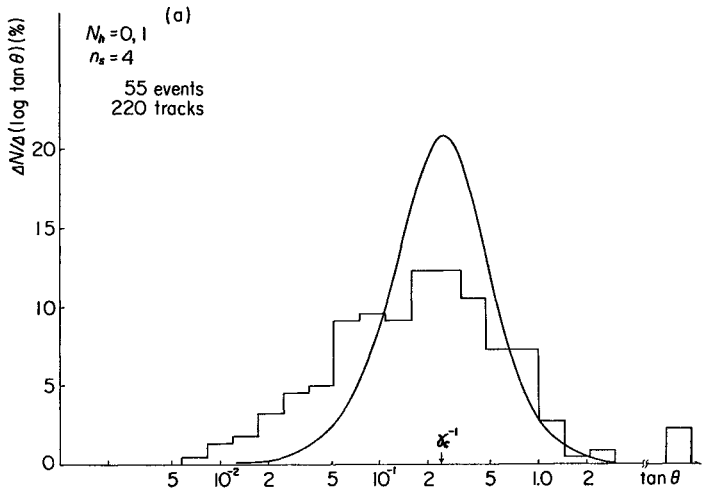

*) For the discussion of angular distribution of $n_s \geq 7$, more 65 events were scanned by the track following method and analysed afterward in order to increase the statistics.

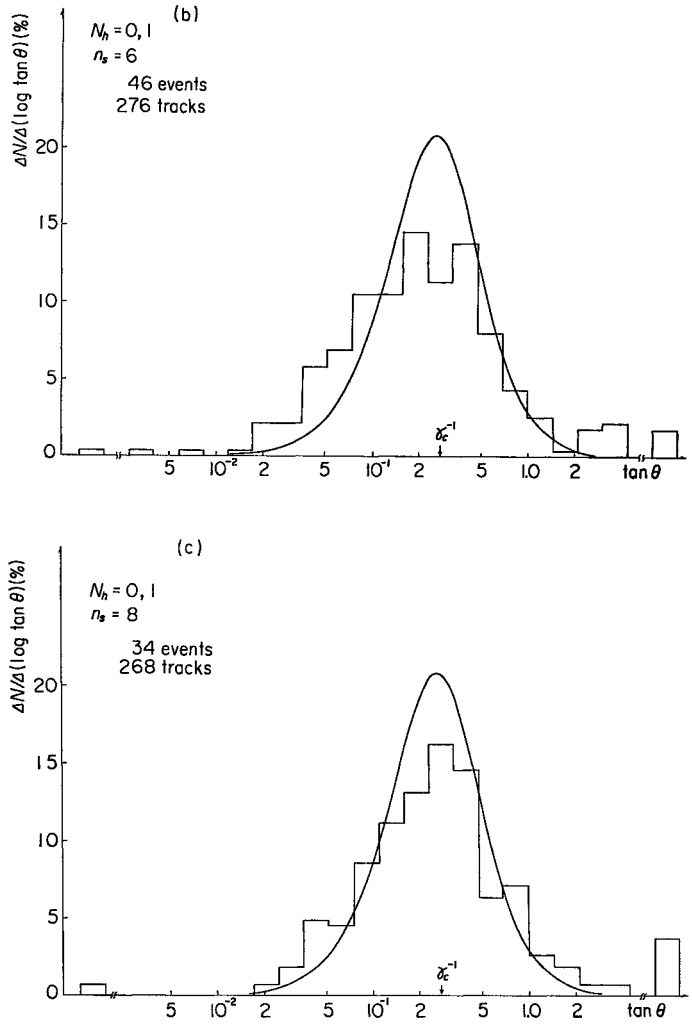

Fig. 6. Differential angular distribution for events with different multiplicities. The smooth curve represents the isotropic distribution in the C. M. S.

in an emulsion nucleus with a certain probability. In this case, most of pions emitted backward in the C. M. S. will have smaller kinetic energy, i.e., 100 $\sim$200 MeV. At such low kinetic energies, the interaction mean free path of pions in the nucleus is so small that pion will suffer a secondary nuclear interaction before leaving the emulsion nucleus, giving rise to a nuclear star with one or more heavily ionizing particles. These events should be out of our criterion ($N_h \leq 1$), and hence be excluded from the data we are concerned in. If the pions are emitted preferably either forward or backward in the C. M. S. in an individual event, the events of backward excess will suffer more an

effect due to the secondary scattering in the nucleus, while the events of forward excess is less affected. In consequence, the composite angular distribution of events with $N_h \leq 1$ is expected to be with forward excess. This is considered to be a case of the smaller multiplicity events. On the other hand, for the case that the pions are emitted in an isotropic way in the C. M. S., the composite angular distribution of events with $N_h \leq 1$ still remains nearly isotropic in the C. M. S., even if some events are excluded by the effect discussed above. This case may correspond to the large multiplicity events. It is needless to say that the composite angular distribution obtained by hydrogen bubble chamber should be symmetric in the C. M. S. for lack of the nuclear effect.

Thus one notices a significant difference in the angular distribution as seen in the fact that the angular distribution is essentially asymmetric in the C. M. S. for the low multiplicity events, while it is nearly isotropic for the high multiplicity events. We now consider more quantitatively nature of the angular distribution, introducing the asymmetry factor[17] Z through

$$Z=(n_f-n_b)/(n_f+n_b), \tag{3}$$

where n_f and n_b are the number of shower particles emitted in the forward and backward direction in the C. M. S., respectively.

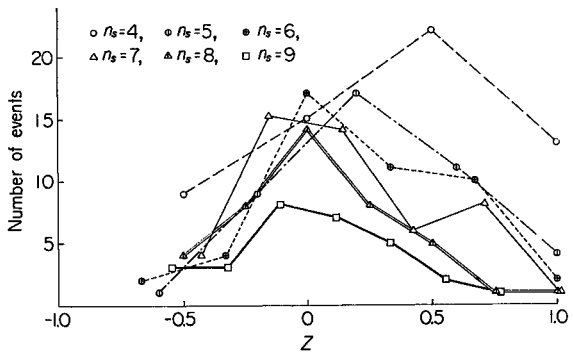

Fig. 7. Distribution of the asymmetry factor, $Z=(n_f-n_b)/(n_f+n_b)$ for events with different multiplicities.

In Fig. 7 plotted is distribution of the asymmetry factor Z for the events with different multiplicities. From inspection of Fig. 7 it is seen that there is a remarkable difference of Z distribution between for the events with $n_s \geq 7$ and for $n_s \leq 6$. For the larger multiplicity events ($n_s \geq 7$) the experimental results are distributed nearly uniform over the wide range of Z from 0.5 to -0.5, while for the smaller multiplicity events with $n_s \leq 6$ there is a significant deficiency of events of negative Z. This forward-excess asymmetry in the small multiplicity events can be explained in terms of statistical fluctuations from the symmetric distribution in the C. M. S. It is also seen that a non-relativistic effect of emitted particles gives only negligible effect in asymmetry of the events.[20]

2-2) *Angular distribution* (2)

Since the difference between the events with $n_s \geq 7$ and with $n_s \leq 6$ is

apparent, we classify the obseved events into four groups (see Table III) in order to study a possible difference in the particle production mechnisms.

Table III. Classifying the observed events.

Group	n_s	$\|Z\|$	No. of events
a	4, 5, 6	≥ 0.5	58
b	4, 5, 6	<0.5	89
c	7, 8, 9, 10	≥ 0.5	21
d	7	<0.5	39
	8	<0.5	25
	9, 10	<0.5	31

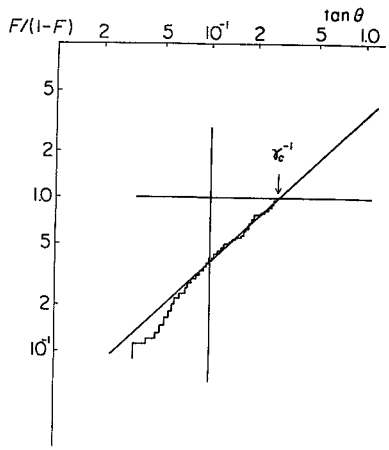

Fig. 8. Duller-Walker plots of the secondary particles emitted in the forward hemisphere in the C. M. S., with $n_s=4$. The straight line is the result obtained by hydrogen bubble chamber. The normalization is taken so that F is 1/2 at $\tan\theta=\gamma_c^{-1}$.

Let us first examine nature of the group of the smaller multiplicity events. At first, we will consider only particles emitted in the forward hemisphere in the C. M. S. in order to minimize the effect of residual nucleus.

In Fig. 8 comparison is made between results of our experiment and of the bubble chamber experiment on the composite integral angular distribution (the Duller-Walker plots)[19] of secondary particles emitted in the forward hemisphere in the C. M. S. taking events with $n_s=4$ as an example. The straight line is the result of obtained by hydrogen bubble chamber.[16] It can be seen from the comparison between the two experimental results that there is a good agreement in the shape of the angular distribution as far as the forward hemisphere is concerned. If we could observe the particles emitted in the backward hemisphere after getting rid of the effect of the residual nucleus, one could expect such resemblance in the angular distribution even in the backward direction.

In order to study the full detail of the angular distribution, we analyze the events of $n_s=4, 5, 6$ dividing them into three groups, $Z\geq 0.5$, $Z\leq -0.5$ and $|Z|<0.5$. The Duller-Walker plots for each group are shown in Fig. 9 and Fig. 10. The smooth curves in broken line drawn in Fig. 9 are theoretical curves obtained by assuming that the fluctuation from an isotropic emission of particles in the C. M. S. yields the asymmetric event, giving the apparent asymmetry factor $Z=0.7$ and -0.54 which is the mean value of Z for the events of $Z\geq 0.5$ and of $Z\leq -0.5$, respectively (for the derivation of this curve, see Appendix A).

If the asymmetric events are due to such a statistical fluctuation, experimental points in the Duller-Walker plots should fall on the theoretical curve. While, as is seen from Fig. 9, the experimental results for both groups, those

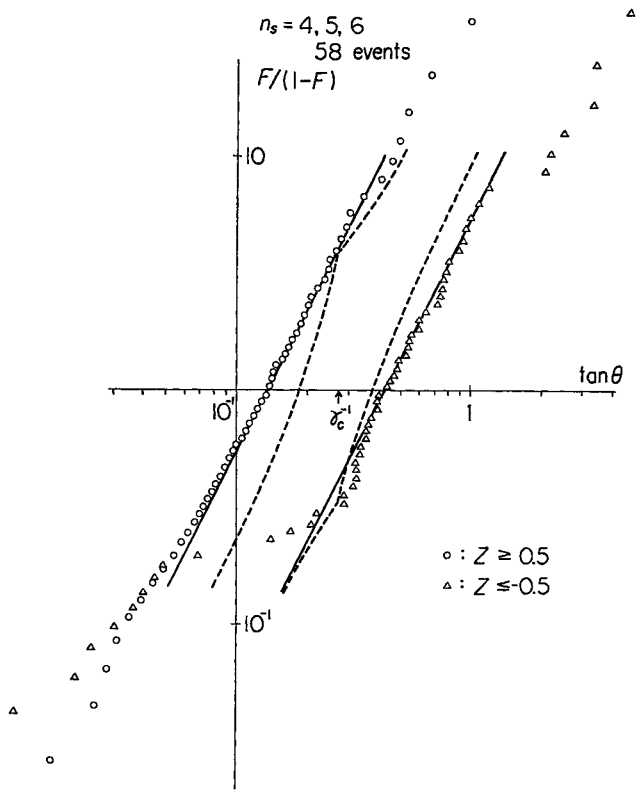

Fig. 9. Duller-Walker plots of the events of $n_s=4,5,6$ for $|Z|\geq 0.5$. The curves in broken line are calculated by assuming that the fluctuation from an isotropic distribution in the C. M. S. yields the asymmetric events, giving the seeming asymmetry factor $Z=0.7$ for $Z\geq 0.5$ and $Z=-0.54$ for $Z\leq -0.5$. The straight solid lines are of slope 2.

with $Z\geq 0.5$ and $Z\leq -0.5$, deviate from the corresponding theoretical curves. Rather they are on straight lines with the slope 2 (solid lines). This implies that the particles are created through isotropic decay of an emitting center moving forward or backward in the C.M.S. The Lorentz factor of this emitting center in the C.M.S., γ_H^*, is estimated from the point where the experimental curve of Duller-Walker plots crosses the abscissa, and one obtains $\gamma_H^*\sim 1.3$. The events of $|Z|\geq 0.5$, therefore, are concluded to be resulted from the isotropic decay of the emitting center moving forward or backward with $\gamma_H^*\sim 1.3$ in the C.M.S.

The Duller-Walker plots for $|Z|<0.5$ are shown in Fig. 10. If the particles are emitted in an isotropic way in the C.M.S. in these events, the Duller-Walker plots must be on a straight line with slope 2, crossing the abscissa at $\tan\theta=\gamma_c^{-1}$. However, that is not the case. The experimental plots show deviation from the straight line with slope 2 (solid line in Fig. 10). We now consider a possibility to interpret the angular distribution of these

events, $|Z|<0.5$, in terms of the emitting center moving with $\gamma_H^*\sim 1.3$ in the C.M.S., the existence of which is established in the asymmetric case, $|Z|\geq 0.5$. Let us assume that the emitting center moves either forward or backward in the C.M.S. with probabilities which are assumed to be proportional to the frequency of events of $Z<0$ and that of $Z>0$, respectively. With this assumption, one is able to construct the expected angular distribution corresponding to a given value of Z. Averaging the results with weight determined by the Z-distribution given in Fig. 7, one obtains the expected total angular distribution based on this model (see Appendix B). The theoretical curve thus obtained is shown in a broken line in Fig. 10, reproducing well the experimental results. Therefore, the events of $n_s=4$, 5 and 6 in the cases of $|Z|>0.5$ and $|Z|\leq 0.5$, are interpreted in terms of one emitting center moving forward or backward with a definite Lorentz factor $\gamma_H^*=1.3$ in the C.M.S.

Next, we examine a group of the larger multiplicity events, $n_s\geq 7$. The Duller-Walker plots for the events of $Z\geq 0.5$ and $Z\leq -0.5$ are shown in Fig. 11 for $n_s\geq 7$. The experimental results agree with the straight line with

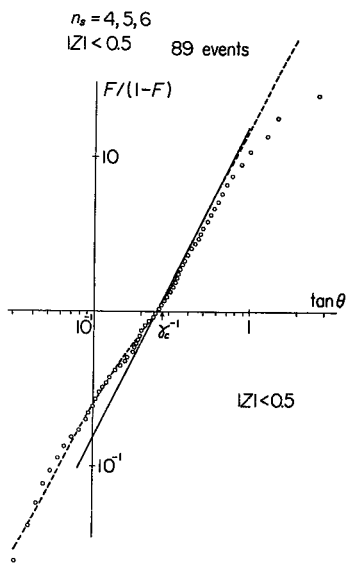

Fig. 10. Duller-Walker plots of the events with $n_s=4$, 5, 6 for $|Z|<0.5$. The straight line with slope 2 corresponds to the isotropic distribution in the C.M.S. The broken line is calculated by assuming the presence of one emitting center moving forward or backward with $\gamma_H^*=1.3$ in the C.M.S.

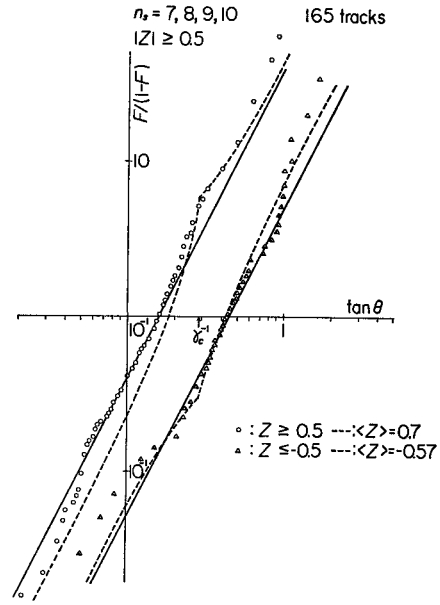

Fig. 11. Duller-Walker plots of the events with $n_s\geq 7$ for $|Z|\geq 0.5$. The straight lines are of slope 2. The broken lines are calculated by assuming that the fluctuation from an isotropic distribution in the C. M. S. yields the asymmetric events, giving the seeming asymmetry factor $Z=0.64$ for $Z\geq 0.5$ and $Z=-0.55$ for $Z\leq -0.5$.

slope 2 (solid lines) which corresponds to the isotropic decay of the moving emitting center, $\gamma_H^* \approx 1.3$. The broken line represents the calculated curves which are obtained under the assumption that the events with $|Z| \geq 0.5$ occur from an isotropic emission of mesons in the C.M.S. by the statistical fluctuation. It seems we cannot exclude, from this figure alone, the possibility that

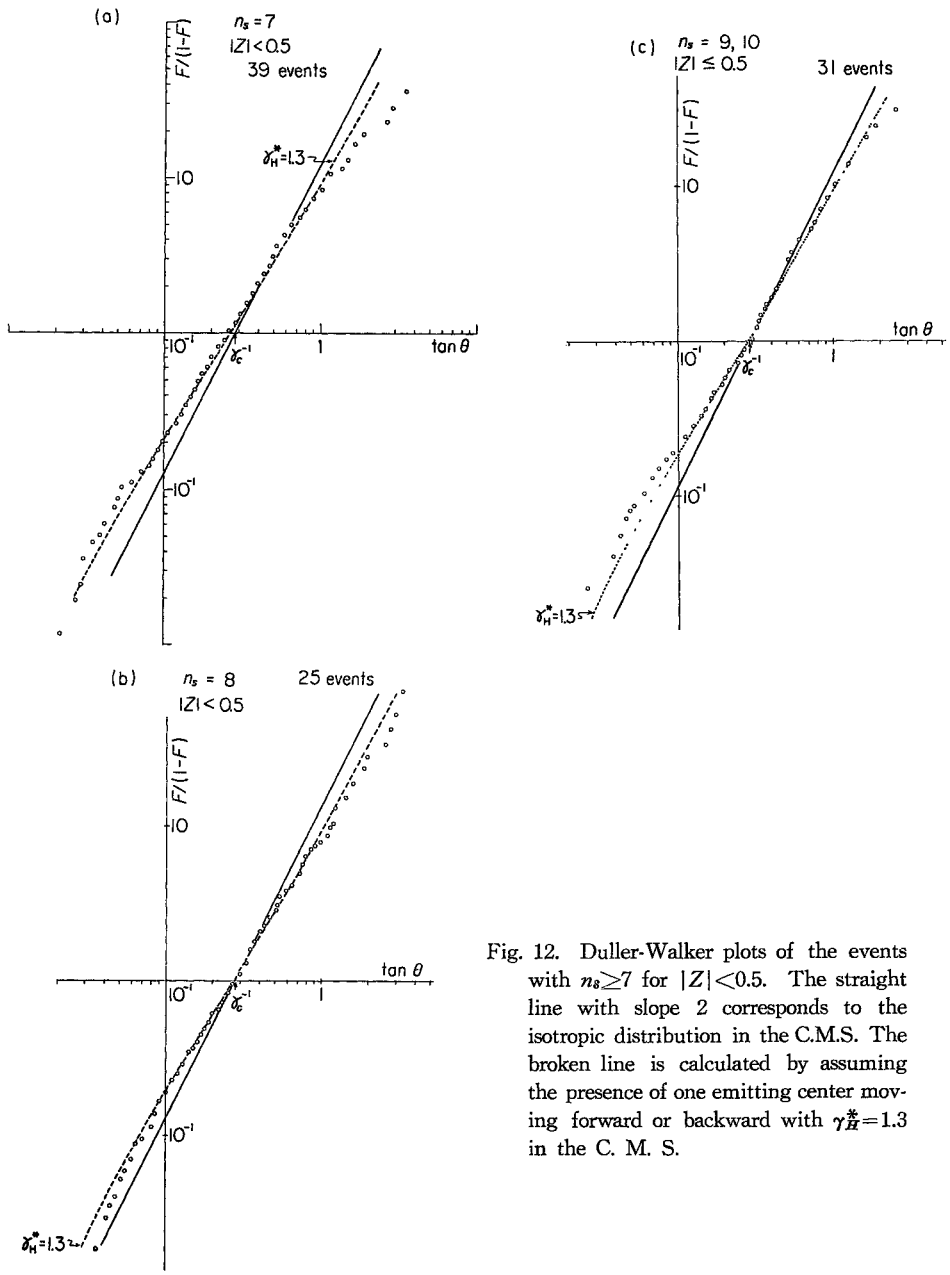

Fig. 12. Duller-Walker plots of the events with $n_s \geq 7$ for $|Z| < 0.5$. The straight line with slope 2 corresponds to the isotropic distribution in the C.M.S. The broken line is calculated by assuming the presence of one emitting center moving forward or backward with $\gamma_H^* = 1.3$ in the C. M. S.

mesons are emitted isotropically in the C.M.S., especially for the events of large multiplicity. However, we consider that a possibility of the isotropic emission of mesons in the C.M.S. is less favoured when one looks at a difference between experimental results and the broken lines, appreciable in the forward hemisphere where the secondary effects in the emulsion nucleus will be least.

The result of the Duller-Walker plots for the events of $|Z|<0.5$ is shown in Fig. 12. A straight line with slope 2 crossing the abscissa near $\tan\theta=\gamma_c^{-1}$ (solid line) does not give the best fit with the experimental results. However, the theoretical curve calculated by assuming the presence of one emitting center moving forward or backward with $\gamma_H^*\approx 1.3$ in the C.M.S. agrees well with the experimental results, as is shown in a broken line in Fig. 12. Therefore, we may conclude that the situation is similar to the case of small multiplicity, $n_s=4$, 5, 6 meaning that the particles are emitted through decay of one emitting center moving forward or backward with the Lorentz factor $\gamma_H^*\approx 1.3$ in the C.M.S. This result is quite important for the conclusion, and it now becomes necessary to study together with the experimental results obtained by a bubble chamber.

The mass of emitting center thus verified is estimated as product of the average number of emitted particles $\langle n_s\rangle$, and their average energy, ε, in the rest system of the emitting center, which is connected with the average transverse momentum P_T, as $\varepsilon=(4/\pi)P_T$. Taking $\langle n_s\rangle\approx 6\sim 7$ and $P_T=350$ MeV/c, we obtain the mass $\mathfrak{M}_H\approx 2.7\sim 3$ GeV, just consistent with the mass of fire-ball observed by emulsion chamber experiment at Mt. Chacaltaya.

Appendix A

We consider a case of n particle emission. Let us express a priori probability of a particle being emitted with an angle between θ^* and $\theta^*+d\theta^*$ in the C.M.S. as

$$f(\theta^*)d(\cos\theta^*). \qquad (A\cdot 1)$$

If there is no correlation between particles, the probability of finding the first particle between θ_1^* and $\theta_1^*+d\theta_1^*$, $\cdots$ the n-th particle between θ_n^* and $\theta_n^*+d\theta_n^*$ is given by

$$dP(\theta_1^*,\cdots,\theta_n^*)=\prod_{i=1}^{n} f(\cos\theta_i^*)d(\cos\theta_i^*). \qquad (A\cdot 2)$$

On the other hand, the angular distribution for such an event is written as

$$g(\theta^*;\theta_1^*,\cdots,\theta_n^*)d(\cos\theta^*)=n^{-1}\sum_{i=1}^{n}\delta(\cos\theta^*-\cos\theta_1^*)d(\cos\theta^*). \qquad (A\cdot 3)$$

From Eqs. (A·2) and (A·3), the average angular distribution is then obtained as

$$\bar{g}(\theta^*)=A\int g(\theta^*;\,\theta_1^*,\,\cdots,\,\theta_n^*)\,dP(\theta_1^*,\,\cdots,\,\theta_n^*). \tag{A·4}$$

If we are concerned with a case where n_f particles are emitted in the forward direction in the C.M.S. ($\cos\theta^*\geq 0$) and n_b particles in the backward direction in the C.M.S. ($\cos\theta^*\leq 0$) among n particles in total, of course $n=n_f+n_b$, the average angular distribution for such a case is given by

$$\bar{g}_z(\theta^*)=A'\int_{\cos\theta_i^*\geq 0,\,\cos\theta_j^*} \cdots\cdots\cdots \int \bar{g}(\theta^*;\,\theta_1^*,\,\cdots,\,\theta_n^*)\prod_{i=1}^{n_f} f(\theta_i^*)\,d(\cos\theta_i^*)\prod_{j=1}^{n_b} f(\theta_j^*)\,d(\cos\theta_j^*), \tag{A·5}$$

where Z is the asymmetry factor, $Z=(n_f-n_b)/(n_f+n_b)$, and A' is the normalization factor given by

$$A'=2^n. \tag{A·6}$$

Here is assumed $f(\theta^*)$ to be symmetirc in the C.M.S.:

$$f(\pi-\theta^*)=f(\theta^*). \tag{A·7}$$

Inserting Eqs. (A·3), (A·6) and (A·7) into Eq. (A·5) yields

$$\bar{g}_z(\theta^*)=\begin{cases}(2n_f/n)f(\theta^*) & \text{for}\quad \cos\theta^*\geq 0,\\ (2n_b/n)f(\theta^*) & \text{for}\quad \cos\theta^*\leq 0.\end{cases} \tag{A·8}$$

Taking into account the definition of Z, we obtain the relation

$$\left.\begin{aligned}2n_f/n&=1+Z\\ 2n_b/n&=1-Z\end{aligned}\right\}. \tag{A·9}$$

From Eqs. (A·8) and (A·9), we finally obtain

$$\bar{g}_z(\theta^*)=\begin{cases}(1+Z)f(\theta^*) & \text{for}\quad \cos\theta^*\geq 0,\\ (1-Z)f(\theta^*) & \text{for}\quad \cos\theta^*\leq 0.\end{cases} \tag{A·10}$$

Further, we now define the integral angular distribution function, $F_z(\theta^*)$, as

$$F_z(\theta^*)=\int_{\cos\theta^*}^{1}\bar{g}_z(\theta^*)\,d(\cos\theta^*). \tag{A·11}$$

If we assume the particle is emitted in an isotropic way in the C.M.S., the distribution $f(\theta^*)$ is given by

$$f(\theta^*)=1/2, \tag{A·12}$$

hence we obtain

$$F_z(\theta^*)=\begin{cases}\dfrac{1+Z}{2}(1-\cos\theta^*) & \text{for}\quad \cos\theta^*\geq 0,\\ \dfrac{1+Z}{2}-\dfrac{1-Z}{2}\cos\theta^* & \text{for}\quad \cos\theta^*\leq 0.\end{cases} \tag{A·13}$$

To convert from the C.M.S. to the Laboratory system we use the following relation:

$$\cos\theta^*=\frac{1}{1+\gamma_c^2\tan\theta}\left[-\gamma_c^2\tan^2\theta\cdot\eta\pm\sqrt{\gamma_c^2\tan^2\theta(1-\eta^2)+1}\right], \qquad (A\cdot14)$$

where θ is the emission angle in the Laboratory system and γ_c is the Lorentz factor of the C.M.S. and η is

$$\eta=\frac{\beta_c}{\beta^*}=\sqrt{\left(\frac{m^2c^2}{(p^*)^2}+1\right)\left(\frac{E_0-Mc^2}{E_0+Mc^2}\right)}, \qquad (A\cdot15)$$

where m and M are the rest mass of pion and nucleon, respectively, p^* is the momentum of pion in the C.M.S. and E_0 is the primary energy of nucleon. Inserting (A·14) into (A·13) yields

$$F_z(\theta)=\begin{cases}\dfrac{1+Z}{2}\left\{1-\dfrac{1}{1+\gamma_c^2\tan^2\theta}\left(\sqrt{\gamma_c^2\tan^2\theta(1-\eta^2)}-\gamma_c^2\tan^2\theta\cdot\eta\right)\right\} & \\ \qquad\qquad\qquad\qquad \text{for}\quad \cos\theta^*\geq 0, & \\ \dfrac{1+Z}{2}+\dfrac{1-Z}{2}\dfrac{1}{1+\gamma_c^2\tan^2\theta}\left(\sqrt{\gamma_c^2\tan^2\theta(1-\eta^2)+1}+\gamma_c^2\tan^2\theta\cdot\eta\right) & \\ \qquad\qquad\qquad\qquad \text{for}\quad \cos\theta^*\leq 0. & (A\cdot16)\end{cases}$$

The final results are obtained

$$\frac{F}{1-F}=\begin{cases}\dfrac{1+t^2(1+\eta)-\sqrt{t^2(1-\eta^2)+1}}{\alpha+t^2(\alpha-\eta)+\sqrt{t^2(1+\eta^2)+1}} & \text{for}\quad \cos\theta^*\geq 0, \\ \dfrac{\alpha^{-1}+t^2(\alpha^{-1}+\eta)+\sqrt{t^2(1-\eta^2)+1}}{1+t^2(1-\eta)-\sqrt{t^2(1-\eta^2)+1}} & \text{for}\quad \cos\theta^*\leq 0,\end{cases} \qquad (A\cdot17)$$

where $t=\gamma_c\tan\theta$ and $\alpha=(1-Z)/(1+Z)$.

Appendix B

Let the Lorentz factor of the emitting center in the Laboratory system be γ. The emission angle of a particle is denoted by $\bar{\theta}$ in the system referred to the emitting center and by θ in the Laboratory system. For a relativistic particle, the following relation holds between them,

$$\gamma\tan\theta=\tan\bar{\theta}/2. \qquad (B\cdot1)$$

We denote the Lorentz factor of the center of mass in the Laboratory system by γ_c. The value of $\bar{\theta}$ corresponding to angle θ defined by $\tan\theta=\gamma_c^{-1}$ is expressed as $\bar{\theta}_c$ and is given by

$$\tan\bar{\theta}_c/2=\gamma/\gamma_c$$

or

$$\cos\bar{\theta}_c = \{1-(\gamma/\gamma_c)^2\}/\{1+(\gamma/\gamma_c)^2\}. \tag{B·2}$$

The asymmetry factor Z is represented as

$$Z=(n_f-n_b)/(n_f+n_b),$$

where n_f and n_b are the number of particles emitted in the forward direction ($\tan\theta<\gamma_c^{-1}$) and in the backward direction ($\tan\theta>\gamma_c^{-1}$) in the C.M.S., respectively.

We now assume that the particles are emitted on an average in isotropic way in the system referred to the emitting center and take into account the effect of the fluctuation in the following approximation. Let us consider an event with asymmetry factor Z with n_f particles in forward hemisphere and n_b particles in backward hemisphere in the C.M.S. Since the half angle θ_c in the C.M.S. corresponds to an angle $\bar{\theta}_c$ in (B·2) in the system referred to the emitting center, we will make an approximation such that n_f particles distribute uniformly in angular region of $\cos\bar{\theta}>\cos\bar{\theta}_c$ and n_b particles in $\cos\bar{\theta}<\cos\bar{\theta}_c$. Then one obtains the following angular distribution in the system referred to the emitting center,

$$f(\cos\bar{\theta};\, Z, \gamma)=\begin{cases}\{1+(\gamma_c/\gamma)^2\}(1+Z)/4 & \text{for } \cos\bar{\theta}>\cos\bar{\theta}_c,\\ \{1+(\gamma/\gamma_c)^2\}(1-Z)/4 & \text{for } \cos\bar{\theta}<\cos\bar{\theta}_c.\end{cases} \tag{B·3}$$

The corresponding integral spectrum takes a form as

$$F(\cos\bar{\theta};\, Z, \gamma)=\int_{\cos\bar{\theta}}^{1} f(\cos\bar{\theta};\, Z, \gamma)\, d(\cos\bar{\theta}). \tag{B·4}$$

Inserting Eqs. (B·1) and (B·3) into Eq. (B·4) one obtains

$$F(\theta;\, Z, \gamma)=\begin{cases}(1+Z)\dfrac{1+(\gamma/\gamma_c)^2}{2}\dfrac{X^2}{1+(\gamma/\gamma_c)^2X^2} & \text{for } X\leq 1,\\ \dfrac{1+Z}{2}+(1-Z)\dfrac{(\gamma/\gamma_c)^2}{2}\dfrac{X^2-1}{1+(\gamma/\gamma_c)^2X^2} & \text{for } X>1\end{cases} \tag{B·5}$$

with

$$X=\gamma_c\tan\theta. \tag{B·6}$$

Denoting the Lorentz factor of the emitting center in the C.M.S. by $\bar{\gamma}$, we obtain

$$\gamma=\bar{\gamma}\gamma_c\pm\sqrt{\bar{\gamma}^2-1}\,\sqrt{\bar{\gamma}_c^2-1}, \tag{B·7}$$

where the sign + (or −) corresponds to the case that the emitting center moves forward (or backward) in the C.M.S. The probability that the emitting center moves forward (or backward) is assumed to be proportional to the number of events for $Z>0$ (or $Z<0$), as was stated in §2-2, and hence can be calculated directly from Fig. 7. For a given Z and $\bar{\gamma}$, the mean

integral spectrum of the angular distribution is given by

$$F(\theta;\ Z, \bar{\gamma}) = P_f F(\theta;\ Z, \gamma_f) + P_b F(\theta;\ Z, \gamma_b), \qquad (B\cdot 8)$$

where γ_f and γ_b are the value of γ corresponding to the cases of the $+$ sign and the $-$ sign in Eq. (B·7), respectively, and P_f (or P_b) the probability that the emitting center moves forward (or backward) in the C.M.S. When Eq. (B·8) is averaged over Z within $|Z|<0.5$ by virtue of the Z-distribution given in Fig. 7, the integral spectra shown in Fig. 10 and Fig. 12 in a broken line can be obtained.

Part II. Analysis of interaction of 10 GeV/c in bubble chamber*)

We have shown in Part I an evidence for the fire-ball creation at the collision of 22.6 and 24 GeV/c proton with a free proton or a quasi-free nuclenon in the nuclear emulsion through analysis of the angular distribution of secondary shower tracks. It was shown that the multiple meson production, especially in the events of n_s greater than four, takes place through production of a single fire-ball with mass of about 2.7 GeV, moving either forward or backward with a Lorentz factor $\gamma_H^*=1.3$ in the C.M.S., and subsequent isotropic decay into mesons.

In this Part II, we shall confirm the results obtained in Part I and proceed to a study of the detailed nature of the fire-ball by analysis of the hydrogen bubble chamber film exposed to 10 GeV/c negative pion. In the hydrogen bubble chamber experiment, we are free from such troubles in analysis that we met in the nuclear emulsion experiment because of the complex nucleus target. Further, the pion interaction is interesting because of being able to see whether there exists a difference between nature of nuclear interaction of a nucleon and of a pion.

The analyzed film contains 1076 pictures by C.B.H. 81**) of Saclay. We concentrated analysis of the events of high multiplicities, $n_s \geq 6$, for a study of the fire-ball among the total of 675 events detected, 90 events of 6, 8 and 10 prongs were measured and analyzed.

It was confirmed that most of secondary mesons are emitted from the fire-ball with mass of 2.4 ± 0.4 GeV, and standard deviation of 0.6 GeV, moving forward or backward with Lorentz factor $\gamma_H^*=1.1$ in the C.M.S. and that the pions produced through decay process of excited baryons occupy only several percent of all secondaries.

The four-momentum transfer of an incident pion and a recoil proton is

*) Shun-ichi Hasegawa, Hirotada Nanjo and Kojiro Tanaka. Science and Engineering Research Laboratory, Waseda University, Tokyo.

**) We express sincere thanks to Prof. Leprince-Ringuet and Prof. C. M. G. Lattes and Prof. Y. Fujimoto for their kind arrangement of C.B.H. 81 films for us.

measured. Their average values are about equal to the nucleon rest energy. This result is consistent with the one obtained from cosmic-ray jet data by Yokoi-Hasegawa formula.

§1. Experimental procedure

Data The data are obtained from 1076 pictures of 35 mm films which were photographed at CERN in 1961. The number of the events is 675 and the multiplicity (n_s) distribution is shown in Fig. 1. We measured and analyzed 6, 8 and 10 prong events among them. The events in which the track length of all secondary particles is shorter than 10 cm are omitted since errors in the momentum measurement are not negligible. Therefore, 75 in 100 six-prong events, 14 in 16 eight-prong events and 1 ten-prong event were measured and analyzed.

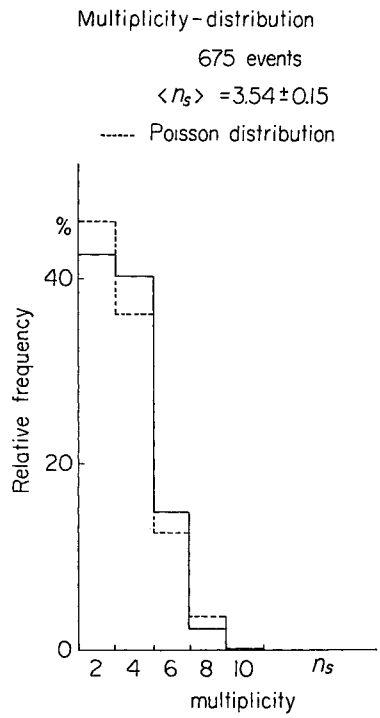

Fig. 1. Multiplicity distribution of secondary particles in 1000 pictures of CBH 81. Total numbdr of events is 675. The average multiplicity $\langle n_s \rangle$ equals to 3.54 ±0.15. The dashed line shows the Poisson distribution centered at average multiplicity $\langle n_s \rangle$.

Optical constant The bubble chamber used in the present experiment is Saclay C.B.H. 81. Though values of all the opitical constants ought to be known, we could not get the precise information, so we had to estimate them. The known constants are the size of the chamber ($32 \times 32 \times 81$ cm), the thickness of glass plates (108.39 mm), the refractive indexes of glass (1.525) and of the liquid hydrogen (1.098), the approximate position of the fiducial marks (the nearest three points make a nearly regular triangle, the side length of which is about 156 mm), and the information with the camera. Six fiducial marks were put on each of two inner surfaces of the front and back glasses, respectively. The relative position of the fiducial marks, the direction of the light axis and the position of the camera, etc., were determined to be consistent with each other by using the 12 fiducial marks on each of the three films.

Measuring method The films are magnified ten times by the projector.*) The track measurement is made selecting four measuring points for incident and secondary tracks including the interaction point. However, three points were selected for the short tracks (<150 mm) and two points for incident tracks of several cm.

The identified bubbles are chosen to be measured on each of three films and the center of the identified bubbles are used as the measuring point. It is possible to check mistakes in measurement by the present method. As a matter of course, the more the measuring points are, the better the accuracy of the track reconstruction is. The number of measuring points is adopted as four including the interaction point in our case, because it was found that accuracy of the track reconstruction in the case of four measuring points is more precise than in the case of three points but not much appreciable, and furthermore the time required for measuring (about three hours for one 6-prong event) is taken into account. The distance between measuring points is kept as long as possible. Each distance between the measuring point and 3 fiducial marks near the measuring point is measured for reconstruction of the track.

Error Errors in reproducing the position in the bubble chamber from the films are caused by the following two reasons. One is error in the measurement of the position on the film. The other is caused by our determination of the parameters of the bubble chamber apparatus, including the optical constants. The latter type of error should not exist in nature, therefore, it must be taken away as much as possible. Necessary parameter values of the bubble chamber apparatus are determined by geometrical consistency of the distances between all possible pairs out of the twelve fiducial marks in total. Accuracy in the parameter determination is limited because of inaccuracy of the measurement of position of the fiducial marks on each one of the films, ± 0.22 mm on the ten times magnified image of the film.

Estimation of the overall errors is made reconstructing the position of the fiducial marks in the following way. The reconstruction of the position is made by measuring its distances to three neighbouring fiducial marks and the results are compared with the previous values determined in a self-consistent way, as described above. The maximum difference between the two determination is found to be $\sim 0.3\%$, namely 1 mm on ten-times magnified image of the film.

In our case, the momentum of incident particle is 10 GeV/c ($\pm 3\%$). Then, if the track length is taken as long as possible, incident momentum should be obtained from the measurement as 10 GeV/c within the relative error of several %, and this is shown in Fig. 2 in which a relation between track length and measured momentum is plotted. Therefore, the error which is caused by determining the optical constants is considered to be negligible,

*) The projector is OLYMPUS OP-560-T.

because error of several % is expected from measuring errors and non-exact uniformity of the magnetic field.

Next, the measurement error is described as follows. Let us denote that a, b, c, d, e and f are fiducial marks, and P is an identified bubble on a secondary track as is in Fig. 3. The distances between P and three neighbouring fiducial marks b, c and d are measured on ten times magnified films. Then, the location of point P is reconstructed numerically on the film using the measured values as follows. Let us draw three circles which have their centers at b, c and d and have each radii equal to the measured distances to P from b, c and d, respectively. Then, the three circles cross with each other. Taking two circles out of the three, we make a triangle connecting the two centers and one of the two cross-points of the two circles, nearest to P. The angles at the cross-points are measured. We define the reconstructing point P' as one of the three cross-points, which has an angle nearest to 90 degrees. The distance R_1 is defined as the one that is measured from P' to the third circle. If the distance R_1 exceeds 1 mm, the measurement is made again. In this way, we can eliminate mistake in the measurement. The average value of R_1 is then obtained as 0.17 mm in our case.

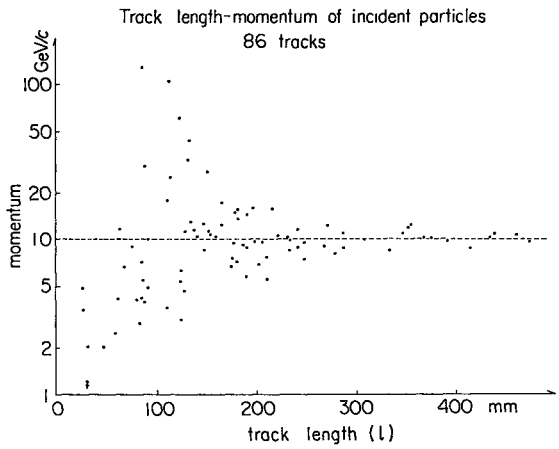

Fig. 2. Track length versus measured momentum of incident 10 GeV/c pion. 86 tracks are plotted.

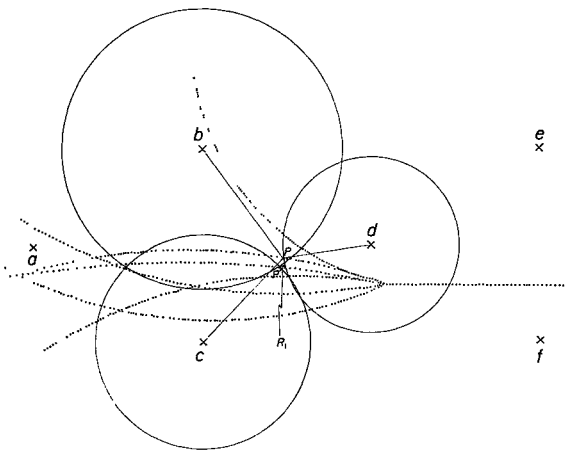

Fig. 3(a). Explanation of our measuring method. Cross marks, a, b, c, d, e and f are the fiducial marks. P is the bubble of which the position should be reconstructed in the chamber. The three circles have their centers at b, c and d, and have each radii equal to the measured distance to P from b, c and d, respectively. P' is the crossing point of two circles b and c, which has an angle $\angle bPc$, nearest to 90°. R_1 is the distance from P' to the third circle.

This reconstructed point on each of three films is projected three-dimensionally into the bubble chamber by the three lines according to the experimental setting. Let us call sum of square of the distances from a certain point in the bubble chamber to the three lines as R_2. We define the three-dimensional position of the bubble as P_2 which shows the minimum value for R_2. When R_2 is larger than 1 mm^2, a re-measurement is made again. Here again we can eliminate mistakes in measurement. Average value of R_2 is obtained as 0.38 mm^2 in our case. This gives a magnitude of the measuring error. It is mentioned in 2-2) that how many such measuring errors cause an error in determination of momentum of the particles.

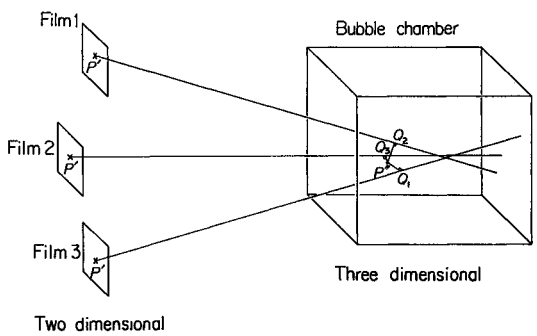

Fig. 3(b). Explanation of reconstructing of the track in a chamber. The point P' on each three films is projected in the bubble chamber. The point P'' that R_2 has the minimum value is decided as the reconstructed point, where

$$R_2=\overline{P''Q_1}^2+\overline{P''Q_2}^2+\overline{P''Q_3}^2 .$$

The third origin of error is caused by the experimental technique. It was reported that the incident pion momentum fluctuates about 3% and the magnetic field in the bubble chamber is not completely uniform, showing the maximum fluctuation of several % around 20 k gauss.

There exist other types of errors described as follows, but all of them are found negligible to the above discussed types. They include errors caused from the fact that a row of bubbles does not always show precisely the trace of a particle, and that the image of a bubble may not be always photographed on the center of the bubble.

Reconstruction program The reconstruction program of tracks is described briefly as follows:

1) Input of the data (measuring values).
2) Determining two-dimensional positions of the measuring points on the filmes.
3) Projecting the three lines through glasses in the chamber.
4) Determining three-dimensional positions of the measuring points in the chamber by minimizing a sum of the square of the lengths of the three perpendiculars from the point to the above three lines.
5) Reconstructing the tracks from positions of the four measuring points.
6) Determining the momenta and emission angles of the particles.
7) Output on physical values of the particles.

§2. Particle identification

1) *Bubble density*

The bubble density (the number of bubbles included in a unit track length) is influenced by variation of temperature and pressure of the liquid hydrogen, which are caused during the working time and also depend on the position in the bubble chamber. The maximum dispersion of the bubble density over the running time and varieties of the position are estimated about 5% and 2% in our measurement, respectively. The statistical error due to the limited number of bubbles is on an average 5% in our case. Then, the resulted error in the measurement of bubble density is estimated about 7% on an average.

Figure 4 shows results of the particle identification using a relation between the normalized bubble density, $b^*(=b/b_0)$, and the momentum, where b_0 and b mean the bubble density of the incident pion and the secondary track concerned, respectively. When the incident track is too short (the statistical error is greater than 5%), average value of the bubble density of the incident tracks in the same picture is taken as b_0.

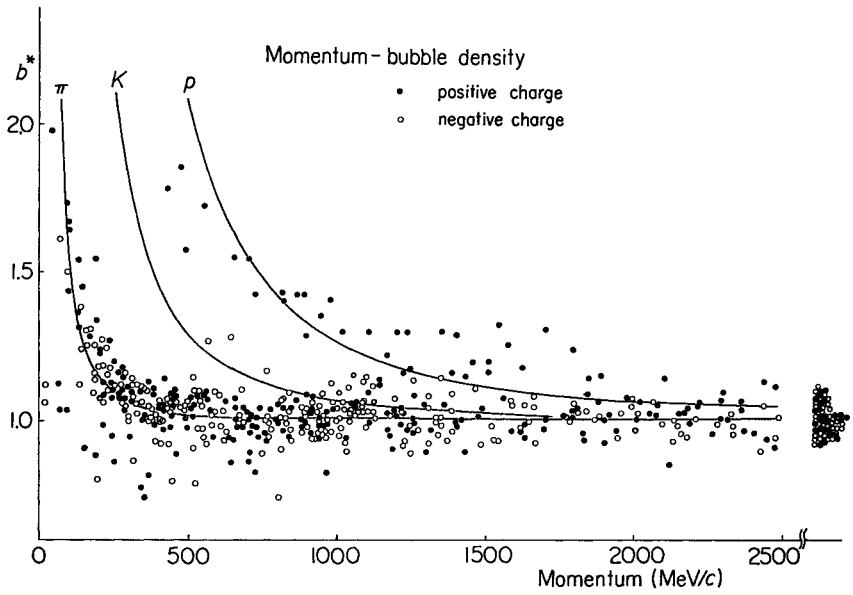

Fig. 4. Relation between the particle momentum (MeV/c) and the normalized bubble density $b^*(=b/b_0)$ where b_0 is the bubble density of the incident 10 GeV/c pion. The solid curves are calculated according to the equation,

$$b^*=b/b_0=(A/\beta^2+B)/(A+B),$$

where β is the velocity of the particle in terms of the light velocity, A is a constant and B is another constant depending on the temperature.

2) *Momentum measurement*

Errors in the momentum measurement depend on the track length and magnitude of momentum of the particles. Table I shows the relative error summarized as a function of track length and momentum. The average value of the track length is 225 mm in our case and tracks longer than 150 mm occupy 82% of the total.

Table I. Relative error in momenta of particles classified by track length and momentum.

Track length (mm) / Momentum (MeV/c)	50~100 (4% in total 2Ry)	100~200 (36% 〃)	200~300 (40% 〃)	300~400 (17% 〃)	400~500 (3% 〃)
0~100			<5		
100~200	≲10	<5	≲5	<5	
200~300	~10	≲5	≲5	≲5	
300~400	~30	~5	≲5	≲5	
400~600	*10	~5	≲5	≲5	
600~800		≲10	~5	≲5	≲5
800~1000		~10	~5	≲5	≲5
1000~1500		~10	≲10	~5	≲5
1500~3000		*10	~10	~5	≲5
Incident track 10GeV/c		*10	~25	~10	~5

3) *Momentum vs. bubble density*

Figure 4 shows a correlation between normalized bubble density and momentum of the particles. The particles are identified by Fig. 4 with use of the expected theoretical relation. The particles of $P \gtrsim 1.2\,\mathrm{GeV}/c$ are out of the range of this method of particle identification.

The particles are also identified by the kinematical method using the energy and momentum conservation in the case of the following modes of the reaction.

$$\pi^- p \rightarrow \begin{matrix} \pi^- p + 4\pi^\pm, & \pi^- p + 4\pi^\pm + \pi^0 \\ \pi^0 p + 5\pi^\pm, & \pi^- n + 5\pi^\pm, \end{matrix} \quad \text{for 6-prong events}$$

$$\pi^- p \rightarrow \begin{matrix} \pi^- p + 6\pi^\pm, & \pi^- p + 6\pi^\pm + \pi^0 \\ \pi^0 p + 7\pi^\pm, & \pi^- n + 7\pi^\pm. \end{matrix} \quad \text{for 8-prong events}$$

The summary of the identified particles is shown in Table II.

It is, in general, difficult to identify the particles which are emitted with very high momenta forward in the C.M.S. In our case, these unidentified particles in the extremely forward direction are assumed as pions and used for the analysis, though some small percentage of the proton contamination may be expected.

Table II. Identified particle number.

	Total track No.	P_L-b^*/b_0		Kinematics	Unknown
8, 10 prongs	122 tracks	e	8	15	23
		π	66		
		K	1	1	
		p	6	2	
6 prongs	450 tracks	e	12	78	100
		π	217		
		K	5	5	
		p	31	2	

§3. Experimental results 1

3-1) *$P_{\parallel}^*$-P_T plots* In Fig. 5 we present the correlation between transverse momentum P_T and longitudinal momentum in the C.M.S. $P_{\parallel}^*$ of emitted particles. Figure (5a) is the plot of P_T vs. $P_{\parallel}^*$ for 8-prong events, 5(b) and 5(c) are those of positive and negative particles for 6-prong events, respectively. The cross mark is for recoil protons and the $\ominus$ mark is for leading negative pions.

One can observe three different groups of the particles in these Figs. 5(a), (b) and (c). The first is the group of negative pions with large $P_{\parallel}^*$ observed in the forward direction in the C.M.S. The second is the group of recoil proton with higher momentum than pions in the backward hemisphere in the C.M.S. The third is the group of the particles other than those above mentioned. This suggests the multiple meson production takes place through the mechanism as follows:

$$(\text{incident } \pi^-) + (\text{target proton}) \rightarrow (\text{surviving } \pi^-) + (\text{recoil nucleon}) + (\text{fire-ball}).$$

Through the following discussion of this section, we shall confirm the mechanism above mentioned and study nature of a fire-ball in details.

3-2) *P_T distribution* The distribution of transverse momentum is shown in Fig. 6. Figures 6(a), (b) and (c) correspond to the 8-prong events, positive and negative pions of the 6-prong events, respectively. The solid curve in Fig. 6 is obtained assuming pions are emitted isotropically through a fire-ball. We assume that the energy spectrum and angular distribution of emitted pions in the rest system of fire-ball is to be represented by the following formula,

$$f(E_f)dE_f d\cos\theta \propto E_f \exp(-E_f/E_0) d^4\boldsymbol{P}\delta(E_f^2-\boldsymbol{P}_f^2-\mu^2), \qquad (1)$$

where E_f, $\boldsymbol{P}_f$ and μ are energy, momentum and mass of a pion, respectively. The distribution of P_T, then, is obtained as

$$f(P_T)dP_T \propto \int_0^\infty P_T \exp(-\sqrt{P_T^2+P_{\parallel}^2+\mu^2}/E_0) dP_{\parallel} dP_T \qquad (2)$$

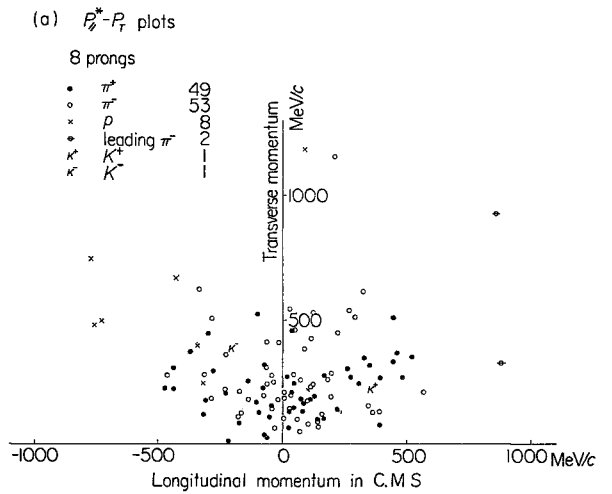

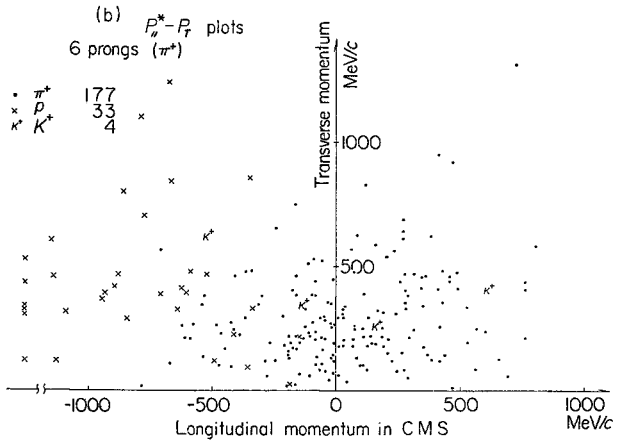

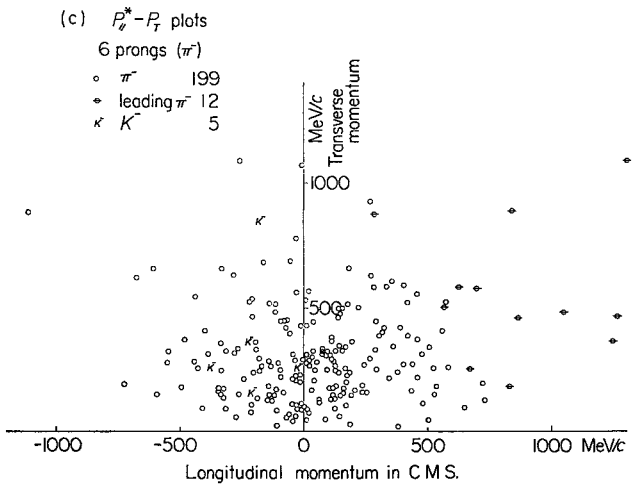

Fig. 5. $P_{\parallel}^{*}$-P_T plot. Figure 5(a) shows in the case of ten 8-prong events. Dark circle is for π^+ meson (49), white circle for π^--meson (53) K^+ for K^+ meson (1) and K^- for K^- meson (1), respectively. Figure 5(b) shows for positively charged particles in 6-prong events. Dark circle is for π^+-meson (177), cross mark for recoil proton and K^+ for K^+-meson (4), respectively. Figure 5(c) shows for negatively charged particles in 6-prong events. White circle is for π^--meson (199), $\ominus$ for leading pion and K^- for K^- meson, respectively.

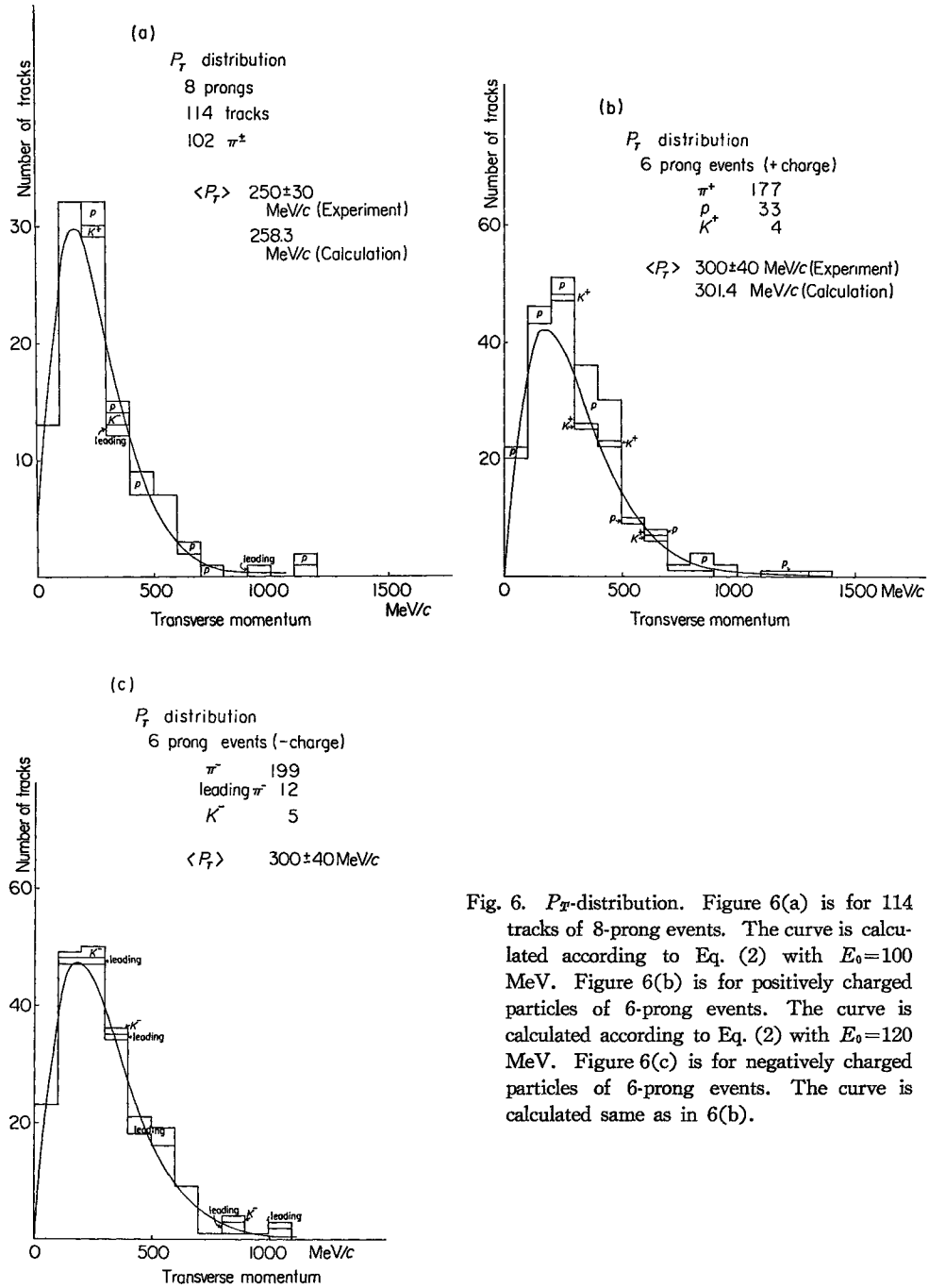

Fig. 6. P_T-distribution. Figure 6(a) is for 114 tracks of 8-prong events. The curve is calculated according to Eq. (2) with $E_0=100$ MeV. Figure 6(b) is for positively charged particles of 6-prong events. The curve is calculated according to Eq. (2) with $E_0=120$ MeV. Figure 6(c) is for negatively charged particles of 6-prong events. The curve is calculated same as in 6(b).

which are shown as solid curves in Fig. 6.

The best fitted values of E_0 with the experimental results are obtained as 100 MeV for the 8-prong events, and 120 MeV for the 6-prong events, respectively. The average values of P_T from the experiment and of calculation by the formula (2) with the best fitted parameter value are shown in the following:

	Experiment	Calculation
$n_s=8$	250 ± 30 MeV/c	258 MeV/c
$n_s=6$	300 ± 15 MeV/c	301 MeV/c

3-3) *$P_{\parallel}^*$ distribution* Longitudinal momentum distribution of emitted pions in the C.M.S., is shown in Fig. 7. Figures 7(a), (b) and (c) correspond to the 8-prong events, and positive and negative pions of the 6-prong events, respectively.

Theoretical $P_{\parallel}^*$ distribution is obtained when we assume that the produced fire-ball moves forward or backward in the C.M.S. in equal probability with Lorentz factor γ_H^* along the incident direction. Using formula (1), we obtain

$$f(P_{\parallel}^*)dP_{\parallel}^* \propto \frac{1}{\gamma_H^*}\{(1+A_1)e^{-A_1}+(1+A_2)e^{-A_2}\}dP_{\parallel}^* , \tag{3}$$

where

$$A_1=\gamma_H^*(\sqrt{P_{\parallel}^{*2}+\mu^2}+\beta_H P_{\parallel}^*)/E_0$$

and

$$A_2=\gamma_H^*(\sqrt{P_{\parallel}^{*2}+\mu^2}-\beta_H P_{\parallel}^*)/E_0 .$$

The results are shown in Fig. 7 for cases of $\gamma_H^*=1.0$, 1.1 and 1.2. The agreement with the experimental data is good in the case of positive pions of the forward direction and negative pions of the backward direction of the 6-prong events, which are not effected by the contamination of the leading negative pion or the recoil proton.

3-4) *P^* distribution* Momentum distribution of particles in the C.M.S., P^*, is presented in Figs. 8(a) and (b) for the case of 8-prong and 6-prong events, respectively. The curves show the result of the calculation according to the following formula,

$$\begin{aligned} f(P^*)dP^* \propto \frac{P^*}{\beta_H^*\sqrt{P^{*2}+\mu^2}} \exp(-\gamma_H^*\sqrt{P^{*2}+\mu^2}/E_0)\Big\{\Big(\sqrt{P^{*2}+\mu^2} \\ -P^*\beta_H^*+\frac{E_0}{\gamma_H^*}\Big)\exp(P^*\beta_H^*\gamma_H^*/E_0) \\ -\Big(\sqrt{P^{*2}+\mu^2}+P^*\beta_H^*+\frac{E_0}{\gamma_H^*}\Big)\exp(-P^*\beta_H^*\gamma_H^*/E_0)\Big\}dP^* \end{aligned} \tag{4}$$

with $\gamma_H^*=1.1$ and 1.2.

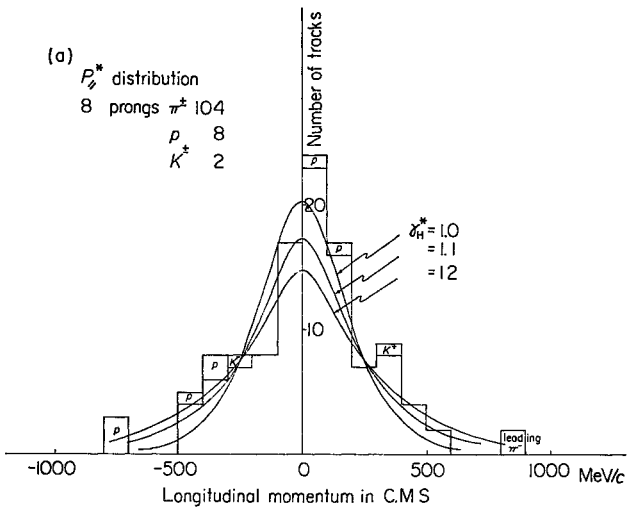

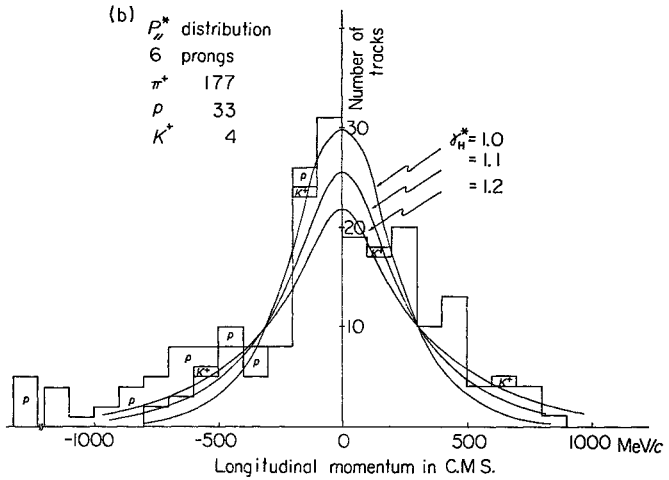

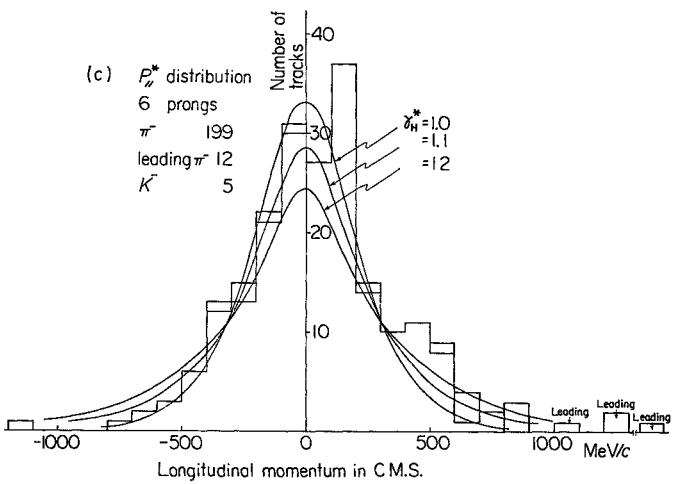

Fig. 7. $P_{/\!/}^*$ distribution. Figure 7(a) is for 8-prong etents. Figure 7(b) is for positively charged particles of 6-prong events. Figure 7(c) is for negatively charged particles of 6-prong events. The curves are calculated according to Eq. (3) with parameters γ_H^* =1.0, 1.1 and 1.2, respectively.

The average values of P^* are summarized in the following.

	Experiment	Calculation
$n_s=8$	325 ± 40 MeV/c	$363(\gamma_H^*=1.1)$
		$392(\gamma_H^*=1.2)$
$n_s=6$	415 ± 20 MeV/c	$416(\gamma_H^*=1.1)$
		$441(\gamma_H^*=1.2)$

The results also show that the fire-ball is produced and moves with $\gamma_H^*=1.1$ in the C.M.S.

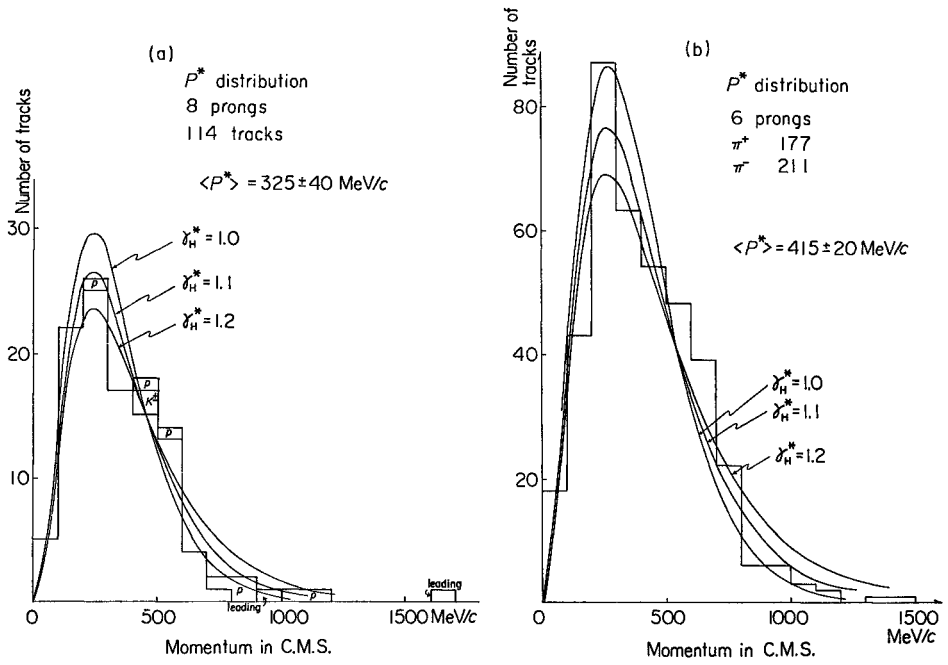

Fig. 8. P^* distribution. Figure 8(a) is for 8-prong events. Figure 8(b) is for 6-prong events. The curves are calculated according to Eq. (4) with parameters $\gamma_H^*=1.0$, 1.1 and 1.2, respectively.

3-5) *$P_{\parallel}^*$-$\langle P_T\rangle$ correlation* Figure 9 shows correlation between longitudinal momentum in the C.M.S., $P_{\parallel}^*$, versus average transverse momentum $\langle P_T\rangle$. The curves correspond to the distribution represented by Eq. (1) with $\gamma_H^*=1.0$, 1.1 and 1.2. The results are consistent with the assumption that the produced fire-ball moves forward and backward in the C.M.S. with $\gamma_H^*=1.1$.

The dip at $P_{\parallel}^*\approx0$ in Figs. 9(a) and (b) are mainly due to isotropy in the decay process.

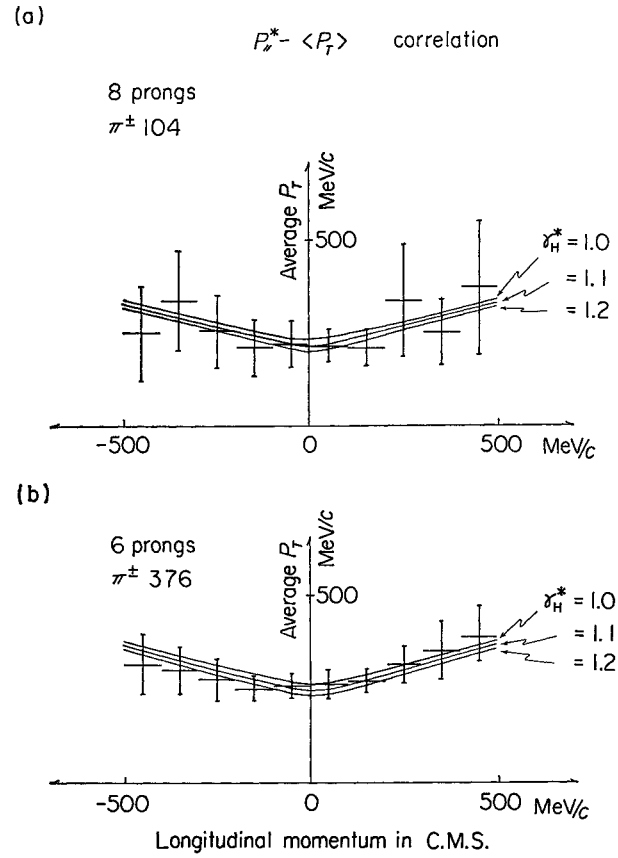

Fig. 9. $P_{//}^{*}$ and $\langle P_T \rangle$ relation. Figure 9(a) is for 8-prong events and Fig. 9(b) for 6-prong events and curves are calculated on the basis of moving fire-ball with Lorentz factor $\gamma_H^*=1.0$, 1.1 and 1.2.

3-6) $\cos\theta^*$-*distribution* In a case where a fire-ball moves with a certain velocity forward or backward in the C.M.S., the angular distribution of produced secondary particles, after taking out a leading pion and a recoil proton, will vary in its shape sensitively depending on assumed volocity of the fire-ball. The experimental results and theoretical curves by Eq. (1) with $\gamma_H^*=1.0$, 1.1 and 1.2 are presented in Fig. 10.

The angular distribution of the 6-prong events agrees well with a theoretical curve with $\gamma_H^*=1.1$. The experimental results of the 8-prong events show a smaller value of γ_H^*, though statistics is not enough to make a definite conclusion.

3-7) *Contamination of excited states* A study is made on the contamination of pions which are produced through the excited baryons of target protons or the excited bosons of incident negative pions. Figures 11(a) and (b) show the histograms of invariant mass of $(p\pi^+)$ and $(\pi^+\pi^-)$ in the 6-prong events,

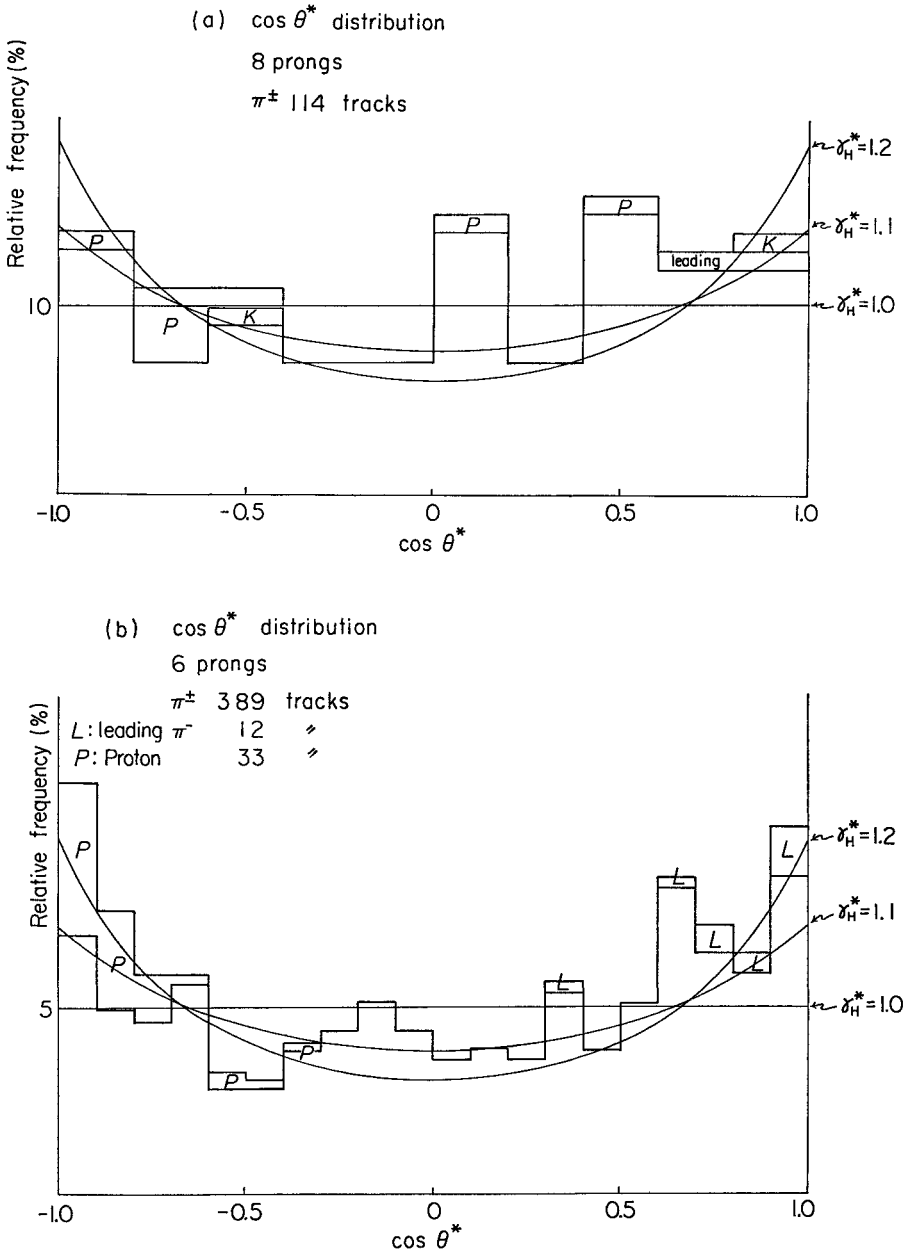

Fig. 10. Angular distribution of secondary mesons in the C.M.S. Figure 10(a) is for 8-prong events. Figure 10(b) is for 6-prong events. The curve is drawn assuming the fire-ball which moves forward and backward with $\gamma_H^*=1.0$, 1.1 and 1.2 and decays into mesons in isotropic way.

respectively. It is evident from these data that several events of N^* (1236) exist among the events in which a recoil proton is identified, and that ρ or f meson scarcely exists. Combination of $(p\pi^-)$ which shows the invariant mass of 1236 MeV is not found. Thus, we may conclude that the contamination of resonance states, as a whole, does not exceed several percent in the total pions of 6-prong events.

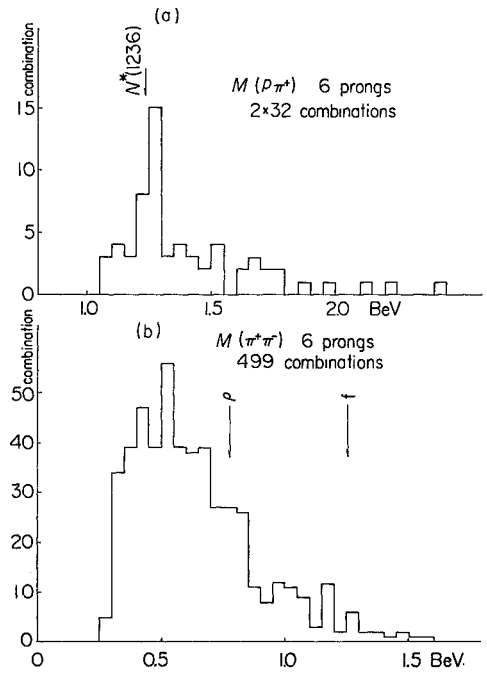

Fig. 11. Figure 11(a) shows invariant mass between recoil proton and a positively charged pion calculated for 6-prong events. 2×32 combinations are made. Figure 11(b) is showing the invariant mass of 499 combinations of $(\pi^+\pi^-)$ for 6-prong events.

3-8) *The $\cos\theta^*$-distribution classified by the momenta of secondary pions* Figures 12(a) and (b) show the angular distributions classified by the momenta of secondary pions, P^*. Figures 12(a) and (b) are $\cos\theta^*$ distribution for secondary pions of $P^*<500$ MeV/c and $500<P^*<1000$ MeV/c, respectively. The curves are the results of calculation assuming a fire-ball moves forward or backward in the C.M.S. in the equal probability with $\gamma_H^*=1.1$. The agreement is quite well. It means almost all secondary pions come through isotropic decay of a fire-ball and contribution from the excited bosons is not appreciable.

3-9) *Mass of fire-ball* In order to determine the invariant mass, $\mathfrak{M}_H$, and Lorentz factor in the C.M.S., γ_H^*, of an individual fire-ball, the events are classified into the following four types.

1) Momentum and energy are conserved without introducing the presence of a neutral particle.
2) Momentum and energy are conserved when one neutral π-meson or neutron is taken into account.
3) Two or more neutral particles are necessary for momentum and energy conservation, though recoil proton and leading pion are identified.
4) The others.

In the cases of 1), 2) and 3), $\mathfrak{M}_H$ and γ_H^* are determined by excluding the recoil proton and leading pion. Table III shows the fire-ball mass obtained from the events which belong to the types 1), 2) and 3), respectively.

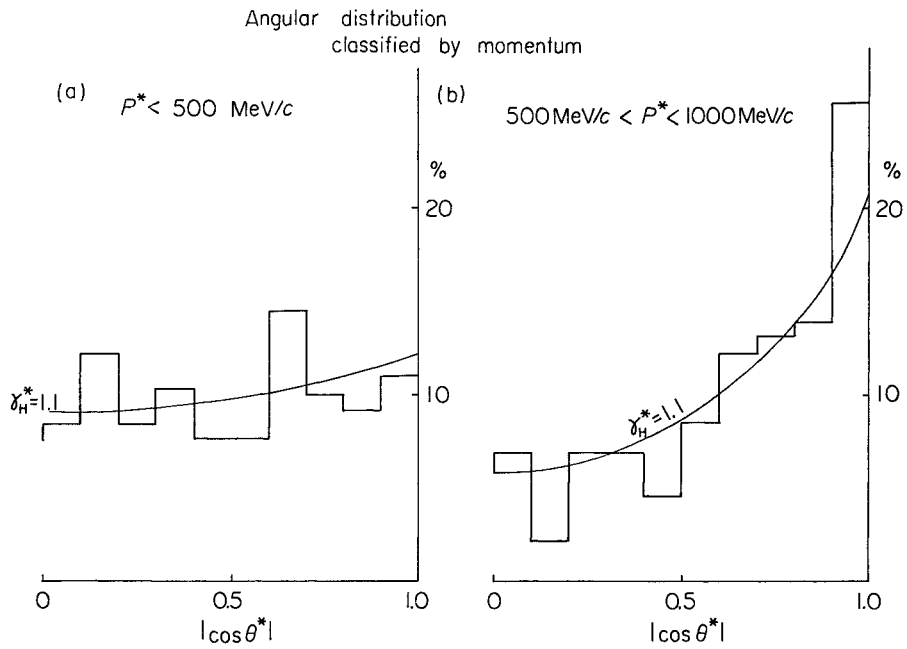

Fig. 12. Angular distribution of secondary mesons classified by its momentum, (a) for $P^*<500$ MeV/c and (b) for 500 MeV/$c<P^*<1000$ MeV/c, respectively. The curve is drawn assuming the moving fire-ball with $\gamma_H^*=1.1$ similarly in Fig. 10.

Table III. Average fire-ball mass classified by decay mode.

N_{ch}	Type	Decay mode	Event No.	$\langle \mathfrak{M}_H \rangle$ (MeV)	Width (MeV)
6	(1)	$p+\pi^-+2\pi^++2\pi^-$	6	1615	$^{+350}_{-260}$
	(2)	$p+\pi^-+2\pi^++2\pi^-+\pi^0$	10	2258	$^{+630}_{-420}$
		$n+\pi^-+3\pi^++2\pi^-$	5	2394	$^{+420}_{-400}$
	(3)	$p+\pi^-+2\pi^++2\pi^-+n\pi^0(n\geq 2)$	9	2247	$^{+430}_{-502}$
	(4)	The others	45		
8	(1)	$p+\pi^-+3\pi^++3\pi^-$	3	2094	
	(2)	$p+\pi^-+3\pi^++3\pi^-+\pi^0$	0	—	
		$n+\pi^-+4\pi^++3\pi^-$	1	2401	
	(3)	$p+\pi^-+3\pi^++3\pi^-+n\pi^0(n\geq 2)$	2	2699	
	(4)	The others	9		
			Average	2180±350 MeV	

In Fig. 13, the histogram of fire-ball mass is shown. The curves are the calculated ones from the phase space prediction of the three-body hypothesis, namely, the assumption of production of leading pion, recoil proton and fire-ball which moves with $\gamma_H^*=1.03$ (Curve a). The curve A will be mentioned in the following chapter. Figure 14 shows correlation of fire-ball mass versus fire-ball Lorentz factor. The dotted line represents the kinematical limit of γ_H^* given by the relation,

$$\gamma_{H(\max)}^*(\mathfrak{M}_H)=\frac{1}{2E_t^*\mathfrak{M}_H}[E_t^{*2}-(M+\mu)^2+\mathfrak{M}_H^2], \tag{5}$$

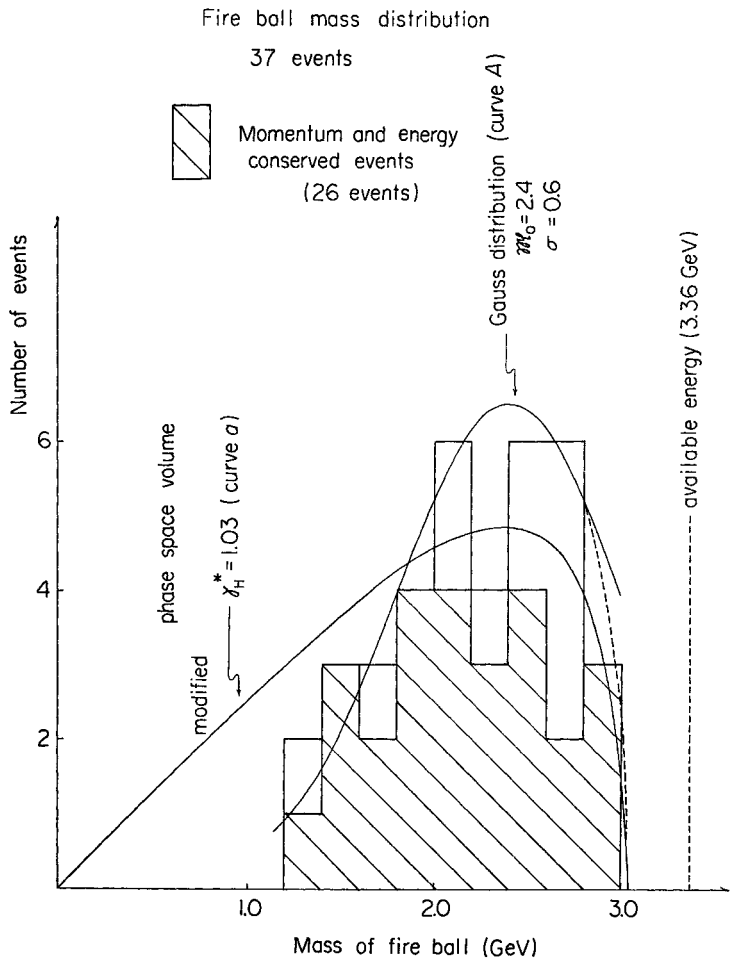

Fig. 13. Fire-ball mass distribution. 37 events are presented in which momentum and energy of all secondary particles are conserved. The drawn curves are explained in the text and Figure.

where E_t^* is the total available energy C.M.S. It is observed that the velocity and mass of fire-ball are suppressed by the phase volume restriction.

§4. Experimental result 2

In oder to study more in detail on nature and production mechanism of a fire-ball, we shall discuss in this section the mass of a fire-ball and magnitude of four-momentum transfer at the collision.

4-1) *Fire-ball mass*

In Fig. 13 of the distribution of fire-ball mass, we present the curve A of Gauss distribution, defined as

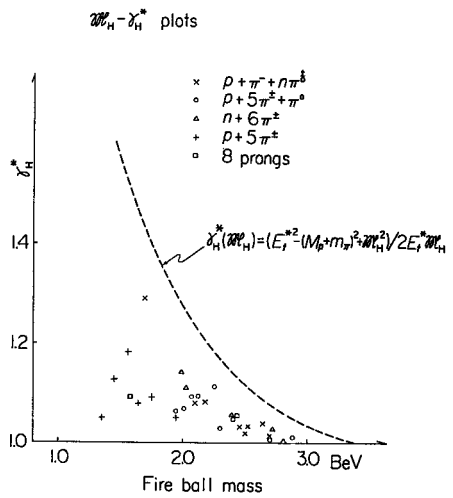

Fig. 14. Relation between $\mathfrak{M}_H$ and γ_H^* are plotted. The dashed line shows the maximum of γ_H^* as the function of $\mathfrak{M}_H^*$ in the given available energy.

$$f(\mathfrak{M}_H)d\mathfrak{M}_H=\frac{1}{\sqrt{2\pi}\sigma}\exp\left(-\frac{(\mathfrak{M}_H-\mathfrak{M}_0)^2}{2\sigma^2}\right)d\mathfrak{M}_H\,, \tag{6}$$

where average mass $\mathfrak{M}_0=2.4$ GeV and standard deviation $\sigma=0.6$ GeV are taken as the best fitted one. The fire-ball mass is obtained as $\mathfrak{M}_H=2.4\pm0.2$ GeV from the peak of the distribution. The arithmetic mean value of fire-ball mass was obtained as $\mathfrak{M}_H=2.2\pm0.35$ GeV as described in Fig. 13. Their difference is considered to be caused by suppression of the fire-ball production of mass greater than 3 GeV by the energy-momentum restriction—the available energy is 3.36 GeV in our case—, while a fire-ball with mass smaller than 1.3 GeV may be cutted off by our criterion, $n_s=6$ and 8. Experimental result agrees with the calculated curve from the phase volume restriction denoted as curve a) in a region where the mass of fire-ball exceeds 2.8 GeV.

The average value of fire-ball mass is also obtained by the following estimate. The total number of pions emitted by the decay of fire-ball, n_t, is obtained from Table III as $n_t=6.0\pm0.5$ for 6-prong events and $n_t=7.5\pm0.5$ for 8-prong events, respectively. On the other hand, it was obtained that the average energy of pion in the C.M.S. is $\langle\varepsilon^*\rangle_6=440\pm20$ MeV for 6-prong events and $\langle\varepsilon^*\rangle_8=380\pm40$ MeV, respectively. By using the following relation,

$$\langle\mathfrak{M}_H\rangle\langle\gamma_H^*\rangle=\langle\varepsilon^*\rangle\langle n_t\rangle, \tag{7}$$

the average values are obtained as

$$\langle\mathfrak{M}_H\rangle_6=2.4\pm0.4\,\text{GeV} \tag{8}$$

and

$$\langle \mathfrak{M}_H \rangle_8 = 2.7 \pm 0.5 \text{ GeV} \tag{9}$$

respectively. These values are consistent with what is obtained from a peak of the Gauss distribution.

4-2) *Four-momentum transfer*

We present in Fig. 15 the four-momentum transfer between incident and surviving pion, $\sqrt{-\Delta_\pi^2}$, as a), and between target proton at rest and recoil proton, including neutron, $\sqrt{-\Delta_p^2}$, as b). The quantity of a recoil neutron is obtained by using the energy and momentum conservation. The average values are given as

$$\sqrt{-\Delta_p^2} = 1040 \pm 200 \text{ MeV} \tag{10}$$

and

$$\sqrt{-\Delta_\pi^2} = 730 \pm 270 \text{ MeV}. \tag{11}$$

One finds that the difference between both the numerical values comes from the mass difference of a proton and a pion. As shown in Fig. 5, the plots of momenta of recoil protons and surviving pions themselves are almost symmetric

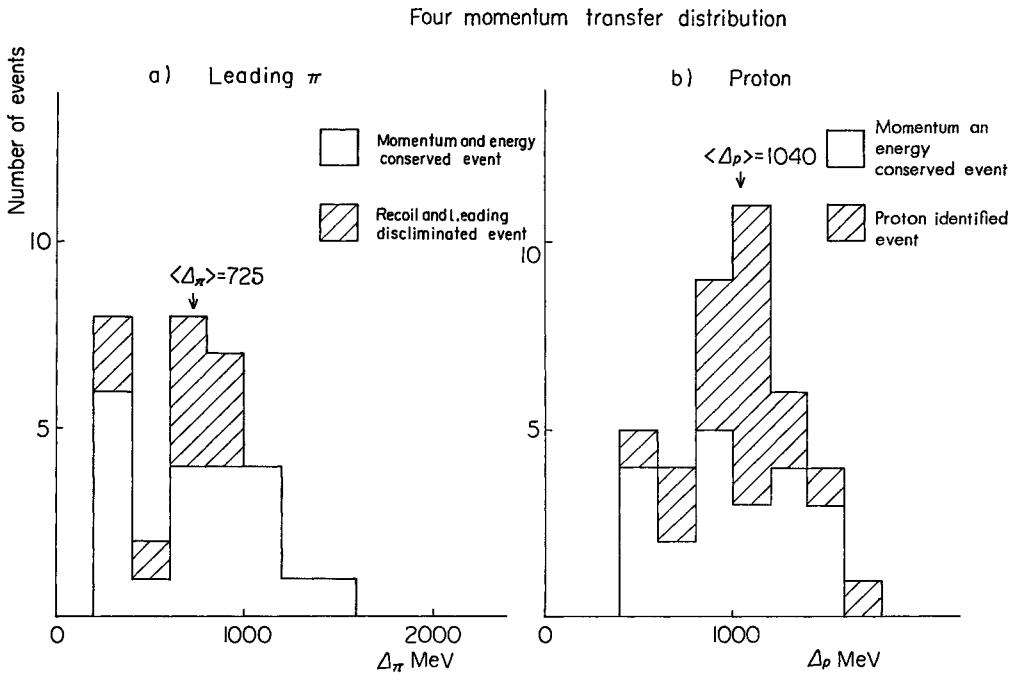

Fig. 15. Four-momentum transfer. Figure 15(a) gives the four-mometum transfer between the incident and the surviving pion and Fig. 15(b) is between target and recoil proton.

in the C.M.S. Since $\sqrt{-\Delta^2}$ is defined in the C.M.S. as

$$\sqrt{-\Delta^2} = \sqrt{(P^*_{\#0}-P^*_{\#})^2+P^2_T-(E^*_0-E^*)^2}, \tag{12}$$

the mass difference between $\sqrt{-\Delta^2_\pi}$ and $\sqrt{-\Delta^2_p}$ is seen to come mainly from the term $(E^*_0-E^*)$ through the mass difference. The experimental values are consistent with this argument.

The distribution of the four-momentum transfer is well expressed by the formula as

$$f(-\Delta^2)d(-\Delta^2) \propto (-\Delta^2)\exp\left(-\frac{(-\Delta^2)}{(-\Delta^2_0)}\right)d(-\Delta^2). \tag{13}$$

Curves of the integral form are given in Figs. 16(a) and (b), together with the experimental data. The values of $-\Delta^2_0$ are given as

$-\Delta^2_0=0.60$ (GeV)^2 for recoil proton

and

$-\Delta^2_0=0.33$ (GeV)^2 for surviving pion.

Twice these values are just the average values of $-\Delta^2$, obtained as

$\langle-\Delta^2\rangle=1.19$ (GeV)^2 for recoil proton,

$\langle-\Delta^2\rangle=0.67$ (GeV)^2 for surviving pion.

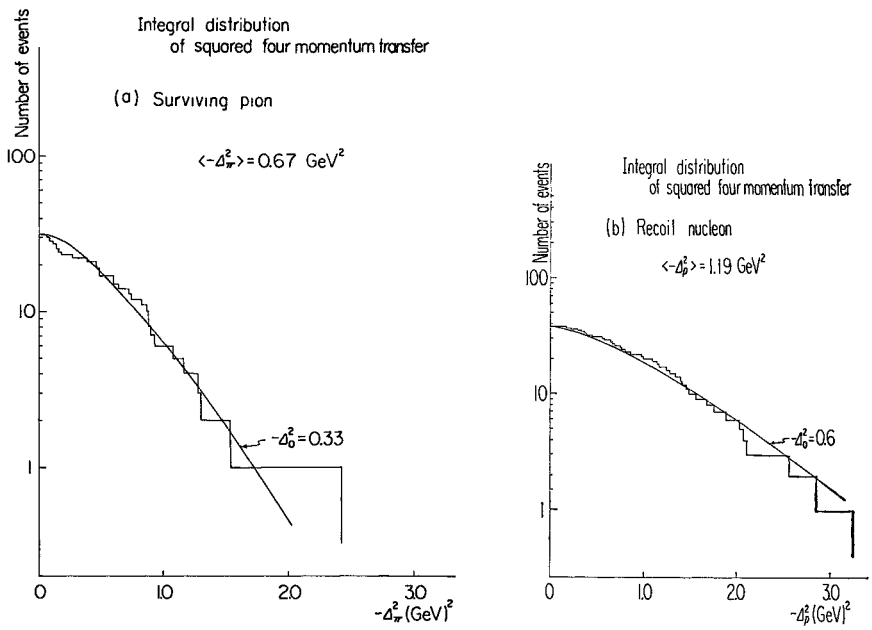

Fig. 16. Integral distribution of squared four-momentum transfer. Figure 16(a) gives squared four-momentum transfer between the incident and the surviving pion and Fig. 16(b) gives between the target and the recoil proton. The curve is given by Eq. (13) with $-\Delta^2_0=0.60$ in Fig. 16(a) $-\Delta^2_0=0.33$ in Fig. 16(b).

4-3) *P_T and $P^*_{//}$ of created fire-ball*

In Fig. 17(a), we present a relation between longitudinal momentum in the C.M.S. and transverse momentum of created fire-ball. In Fig. 17(b) we show the same relation of recoil nucleon and surviving pion. The angular distribution in the C.M.S. of created fire-ball is shown in Fig. 18. From these one observes forward abundance in the creation of fire-balls. This tendency, however, is explained by the selection bias of the events, for which energies and momenta of the secondary particles are conserved, and the recoil proton and the surviving pion are also identified together. The numbers of particles emitted forward and backward are 118 and 89, including π^0 mesons and neutrons, respectively, in the selected events. While they are 115 and 137 in

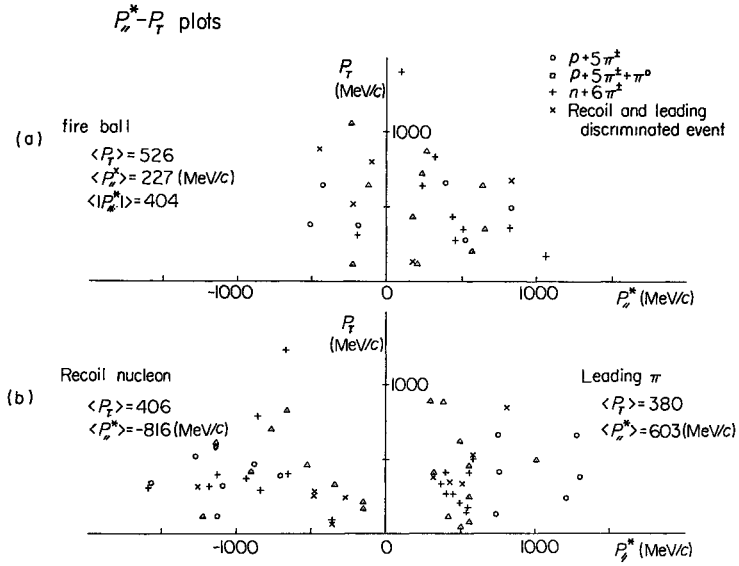

Fig. 17. $P^*_{//}$-P_T relation of created fire-ball in (a), and recoil nucleon and surviving pion in (b).

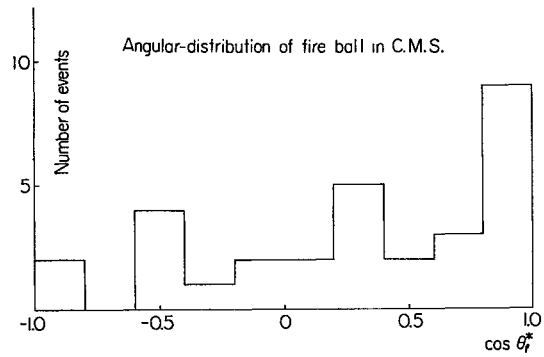

Fig. 18. Angular distribution of created fire-ball in the C.M.S.

the remaining events, respectively. Sum of both is consistent with assumption of the symmetrical emission of fire-ball in the forward and backward hemisphere.

4-4) *Inelasticity*

If the multiple meson production takes place through the three-body mechanism, a surviving pion, a recoil proton and a fire-ball, the inelasticity has its meaning even in our energy and it is analyzed as shown in Fig. 19. The distribution has a peak around $K\sim0.7$. The mean values are obtained as

$K=0.69\pm0.055$
for 6-prong events

and

$K=0.76+0.1$
for 8-prong events.

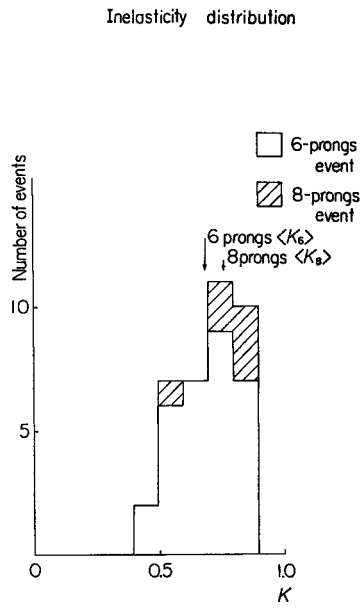

Fig. 19. Distribution of the inelasticity.

Part III. Conclusion and discussion

We have analyzed the nuclear interaction of 22.6 and 24 GeV/c proton in nuclear emulsion in Part I, and of 10 GeV/c negative pion in the hydrogen bubble chamber (C.B.H. 81) in Part II. Let us here summarize briefly the conclusion which we have arrived at by these analyses, and discuss a general feature of the high energy nuclear interaction including the results of the accelerator experiments and the cosmic-ray experiments obtained by foreign laboratories.

§1. Summary of our results

Our main results are summarized as follows. Secondary mesons, especially in events of large multiplicity, are emitted through the intermediate state—called a fire-ball—which moves with a certain velocity forward or backward in the C.M.S. The fire-ball production was observed in both cases of incident proton and pion and we could not observe any difference between the different kinds of incident particles. Then, the interaction mechanism is described as follows,

Incident particle (p or π) + target (p)
→ surviving particle (p, n, or π) + recoil nucleon + fire-ball.

The contribution of an excited state, resonance, of a baryon and a boson known up to date is quite limited, several % of secondary mesons in events of $n_s=6$ and 8 in our analysis of hydrogen bubble chamber of 10 GeV/c pion.

1-a) *Mass* The mass of fire-ball was measured for the events in which the momenta and energies are conserved among secondary particles. It is an invariant mass of all the secondary particles in the event after taking out its surviving pion and recoil nucleon. An average value of the mass of fire-ball was obtained as 2.4 ± 0.2 GeV. This value of fire-ball mass is consistent with the one estimated from the 22.6 and 24 GeV/c proton interaction experiment, by using the mean multiplicity and the mean transverse momentum.

1-b) *Momentum distribution of secondary mesons* Mesons are emitted isotropically and their momentum distribution is of exponential form in the rest system of a fire-ball, and it is described as

$$f(E_f, \cos\theta)dE_f d\cos\theta \propto E_f P_f \exp(-E_f/E_0)dE_f d\cos\theta$$

with

$E_0=120$ MeV for 6-prong events,

$E_0=100$ MeV for 8-prong events.

1-c) *Motion of fire-ball* Lorentz factor of a fire-ball in the C.M.S. was measured and obtained as $\gamma_H^*=1.3$ for 22.6 and 24 GeV/c proton case and $\gamma_H^*=1.1$ for 10 GeV/c negative pion case. The difference of these results will be explained on the basis of kinematical restriction caused by the available energy. (See discussions in §3.)

1-d) *Momentum transfer* A characteristic quantity of the fire-ball creation is observed in the four-momentum transfer between an incident particle and a surviving particle, and between a target particle and a recoiled particle. In our analysis of 10 GeV/c negative pion, it was observed that the distributions of $-\Delta_\pi^2$ and $-\Delta_p^2$ have the same form as

$$f(-\Delta^2) \propto (-\Delta^2)\exp\left(-\frac{(-\Delta^2)}{(-\Delta_0^2)}\right)d(-\Delta^2),$$

with $-\Delta_0^2=0.60$ (GeV/c)^2 for proton and $-\Delta_0^2=0.33$ (GeV/c)^2 for pion. The average value is given by twice of $(-\Delta_0^2)$. These values are essentially different from the one in peripheral phenomena, for example, production of resonance states.

1-e) *Mass distribution* We can consider two possibilities about nature of a fire-ball. One is to assume that the fire-ball is a group of a large number of heavy boson states like the giant resonance in the nuclear reaction. Another is to assume that it is a new state of matter having a unique mass value. If we consider here the latter case, we are able to estimate the life-time of

the fire-ball in a meaning of the correspondence theory by the Breit-Wigner formula. Figure 20 shows a comparison of the fire-ball mass distribution with the Breit-Wigner formula defined as

$$f(\mathfrak{M}_H)d\mathfrak{M}_H \propto \frac{(\Gamma/2)^2}{(\mathfrak{M}_H-\mathfrak{M}_0)^2+(\Gamma/2)^2},$$

where $\mathfrak{M}_0=2.4$ GeV and $\Gamma/2=0.8$ GeV are taken as the best fitted parameter values. Then the life-time, T, which corresponds to the width of the mass distribution here obtained, is calculated and it gives

$$T=4\times10^{-25}\ \text{sec.}$$

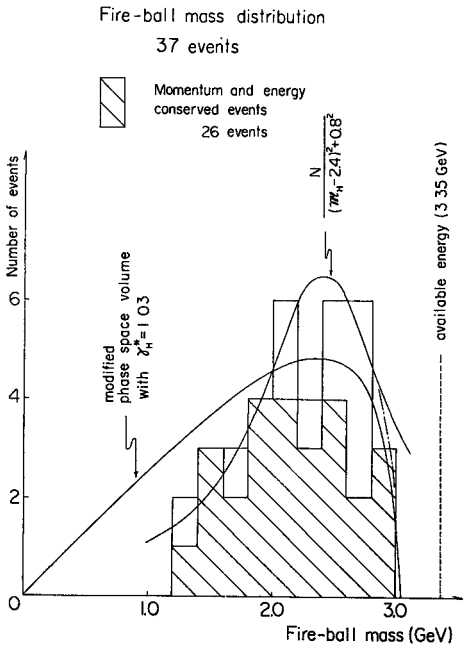

Fig. 20. Comparison of the fire-ball mass distribution with Breit-Wigner formula.

§2. Comparison with other experiments

Let us now study whether nature of fire-ball is changing by the incident energy or different kind of incident particles, proton and pion, or not. For this purpose, we will compare our results with those obtained by other authors. They are from the following cosmic-ray experiments:

Cloud chamber study: $E_0=100\sim400$ GeV [21),35)]
Emulsion stack analysis: $E_0=1\sim10$ TeV [22)]
Emulsion chamber study: $\sum E_\gamma=3\sim20$ TeV [23)]

and from the following accelerator experiments, proton interactions in bubble chambers and in nuclear emulsion.

$$E_p=14,^{24)}\ 19.8,^{25)}\ 23.5,^{26)}\ 24 \text{ and } 28.5\ ^{27)}\ \text{GeV}/c.$$

π-meson interactions in bubble chambers and in nuclear emulsion.

$$E_\pi=6.1,^{28)}\ 8,^{29)}\ 10,\ 16,^{30),31)}\ 25\ ^{32)} \text{ and } 60\ ^{33),34)}\ \text{GeV}/c.$$

2-a) *Mass* The result of emulsion chamber exposed to cosmic-rays[23)] confirmed the existence of a fire-ball and a part of the rest energy given to γ-rays

was found to be 1.3 ± 0.2 GeV in an average. The energy range of the observation extends from $\sum E_\gamma = 3{,}000$ GeV to 50,000 GeV. They estimated from the above value the total rest energy as 2 to 3 GeV, assuming the charge independence of π-mesons and taking into account of their experimental condition. The comparison with our result of 2.4 ± 0.2 GeV tells us that the present experimental data are consistent with a hypothesis of production of a fire-ball of constant mass of about 2.5 GeV from 10 GeV up to around 100,000 GeV of an incident energy. There are several cosmic-ray experiments providing information on the fire-ball in the intermediate region of this wide energy range. As will be seen in discussions in an accompanied paper, all of the experiments are also consistent with the constant mass hypothesis.

In order to see more details in the accelerator energy regions, we present in Fig. 21[21),24),25),27),28),31),32),33)] fraction of the events with prong number n_s as a function of an available energy in the collision. We will discuss whether this change can be consistently interpreted by hypothesis of a fire-ball production of the constant mass, $\sim$2.5 GeV.

First, one notices the fraction of $n_s=6$ does not change appreciably with the available energy beyond 5 GeV. From the assumed constant value, 2.5

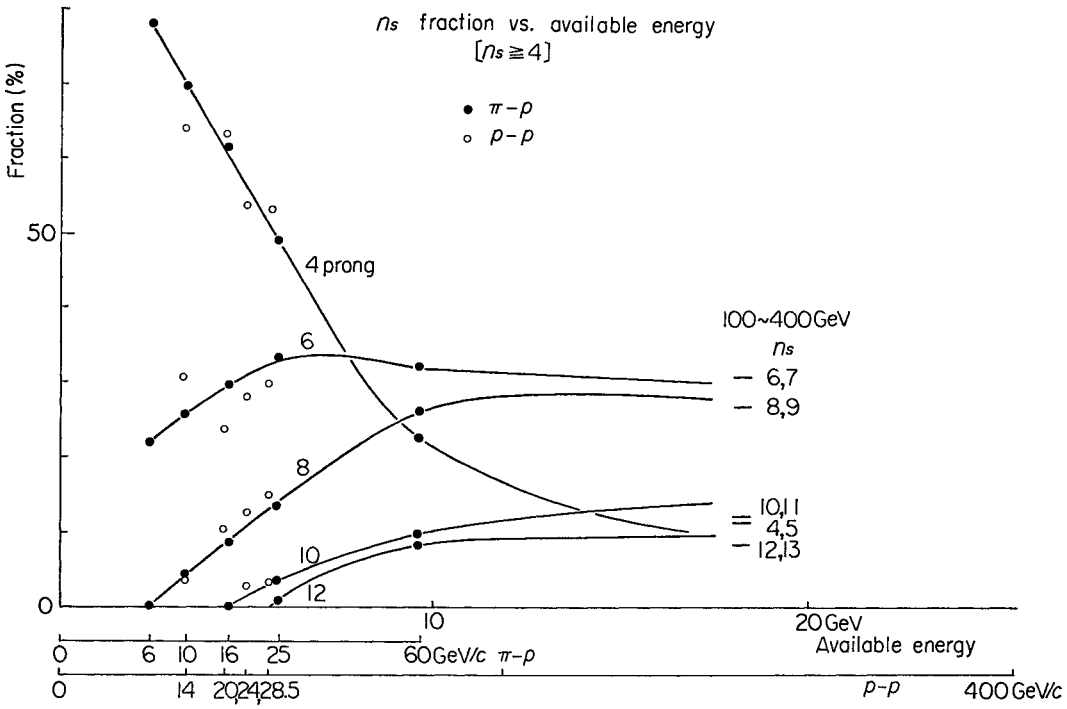

Fig. 21. Relation between n_s fraction and available energy. White circle is for p-p interaction, dark circle for π-p interaction and—mark for 100~400 GeV cosmic-ray data. Solid curve is hand-writing.

GeV, for its rest mass, the events of $n_s=6$ will occupy a major part of the single fire-ball production. Therefore, the experimental points can be interpreted as that the main channel of the interaction is the one fire-ball production as the available energy exceeds 5～10 GeV. A decrease of the fraction below 5 GeV is consistent with the expected one from the energetics with the fire-ball mass, 2.5 GeV.

Second, one sees a rapid decrease of the fraction of $n_s=4$ at several GeV region. The production of resonance states of a baryon and a boson will be responsible for the events of $n_s=4$, so that it shows that the channel of the production of resonances decreases with the increase of incident energy and the fire-ball production is going to be the dominant process in the high energy inelastic nuclear interaction. Indeed, in our analysis of emulsion stack of 22.6 and 24 GeV/c proton, we observe two types of angular distributions for $n_s=4$. One is the type that, of the four tracks, two appear strongly collimated in the forward direction and the other two in the backward, or sometimes one in the forward and the other three in the backward, and vice versa. The other is the type of near isotropy consistent with the angular distribution of the fire-ball.

Third, an increase of the fraction of $n_s\geq 8$ can be interpreted by the two possibilities. One is an effect of the mass distribution of the fire-ball, which has a half-width of about 800 MeV. Due to the kinematical relation, a fire-ball of smaller mass in the distribution will be produced more frequently in the events of smaller available energy. The other is that the increase of incident energy opens a channel of the production of two fire-balls of the same constant mass when the energy exceeds the threshold. In 60 GeV/c pion of Serpukhov experiment, therefore, the production of two fire-balls will not be negligible.

2-b) *Momentum distribution* In Fig. 22, we present the momentum distributions of secondary pions in the fire-ball system by 10 GeV/c and 16 GeV/c[30] incident pion and 100～400 GeV/c incident proton in cosmic-rays observed by Dobrotin et al.,[21] respectively. All are well represented by an exponential type distribution as described in Fig. 22 and one cannot observe any detectable difference among them.

2-c) *Motion of fire-ball* The angular distribution of secondary mesons reflects sensitively the velocity of the fire-ball. In Fig. 23(a), we present the angular distributions of secondary pions in the forward hemisphere in the C.M.S. for the events of $n_s\geq 6$ by incident negative pions of 10 GeV/c, 16 GeV/c,[31] 25 GeV/c[32] and 60 GeV/c.[33] As is seen in Fig. 23(a), each of the angular distributions is well represented by a curve calculated on the basis of isotropic decay into mesons of a fire-ball moving with a Lorentz factor in the C.M.S. of a certain value depending on the incident energy. It seems that the Lorentz factor in the C.M.S. increases with the incident energy. It reaches $\gamma_H^*=1.4$ at 60 GeV/c pion.

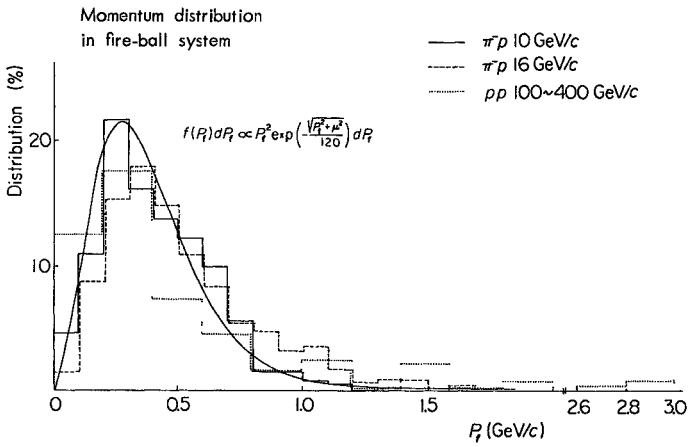

Fig. 22. Momentum distribution of secondary mesons in the rest system of fire-ball. The data are taken from π^--p 10 GeV/c, p-p 100 ~ 400 GeV. The distribution of π^--p 10 GeV/c is the one of momentum in the C.M.S., because of little difference in the case of $\gamma_H^*=1.1$.

The angular distributions of the proton interactions are now examined. In Fig. 23(b), we present the angular distribution of secondary mesons by the incident proton of the accelerator experiment with momentum of around 25 GeV/c,[16),26)] and of the cosmic-ray experiment with energy of around 100~1000 GeV.[35)] The best fit gives $\gamma_H^*=1.3\sim1.4$ for both cases.

2-d) *Four-momentum transfer* There are not many analysis on the four-momentum transfer in the production of a fire-ball. Yokoi and one of us (S.H.) made a formula to obtain magnitude of the four-momentum transfer between the neighbouring fire-balls from the angular distribution data of jet showers. In Fig. 24, we present their result of the analysis applied to the Texas loan stack data[22)] of the Chicago group. The average value is

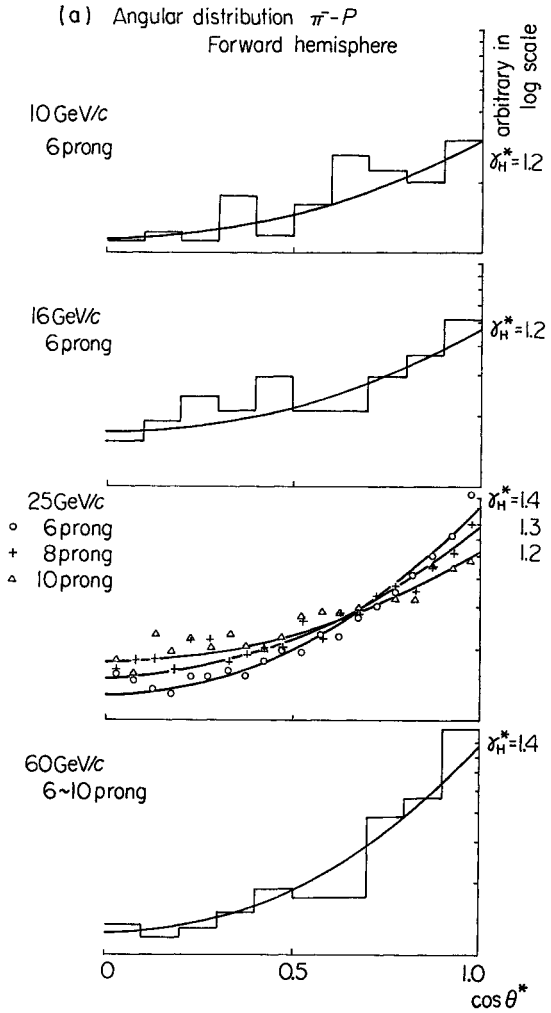

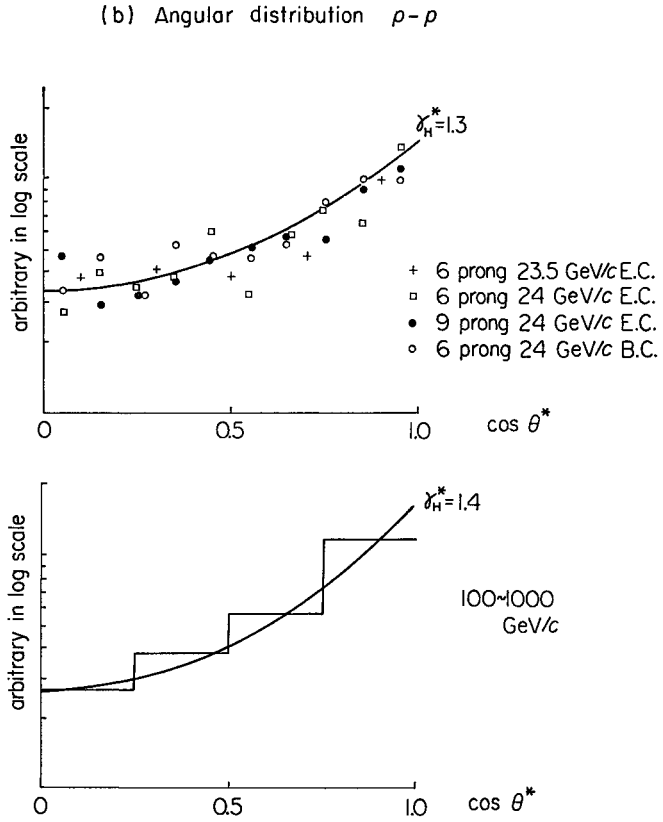

Fig. 23. Angular distribution of secondary mesons in the forward hemisphere. Figure 23(a) shows 6-prong events of 10 GeV/c and 16 GeV/c and 6, 8, 10 prongs of 25 GeV/c and 6 to 10 prongs together of 60 GeV/c. Figure 23(b) shows for p-p interaction 24 GeV/c and cosmic-ray data. The curves are drawn assuming the isotropic decay from fire-ball moving with $\gamma_H^*=1.2\sim1.4$.

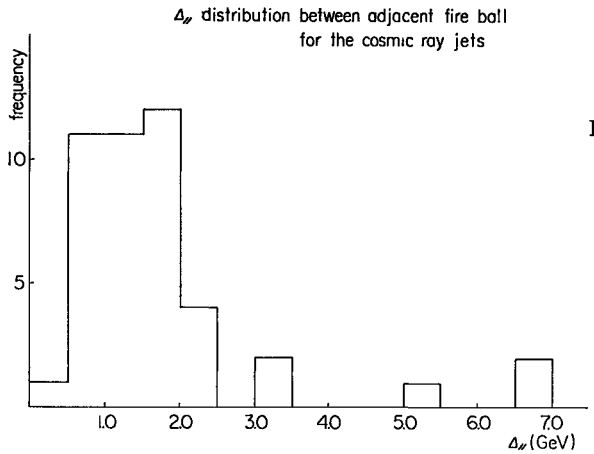

Fig. 24. $\Delta_{//}$ four-momentum transfer from the longitudinal components between adjacent fire-ball for the cosmic-ray jets of Texas loan stack, calculated by using Hasegawa-Yokoi formula.

$\sqrt{-\Delta^2}=1\sim2$ GeV, which can be compared with the present results of $\sqrt{-\Delta_\pi^2}=0.73$ GeV and $\sqrt{-\Delta_p^2}=1.04$ GeV for the 10 GeV π^--meson experiment.

§3. Comparison with *H*-quantum theory

The H-quantum theory was proposed in 1961 by one of us (S.H.) through the analysis of jet-shower data in the emulsion stacks. The theory proposes the existence of the H-quantum which is an energy quantum in the process of multiple production of mesons, and its rest energy is given as two to three times of the nuclear rest energy. He also proposes the velocity quantization rule in the production process of the H-quantum. This is expressed as the Lorentz factor in C.M.S. being constant, $\gamma_H^*\approx1.4$ for the first created H-quantum. We will discuss here whether the available experimental data are supporting the theory or not.

Constancy of the mass is seen, in a large scale, in comparison of our data of 2.4 ± 0.4 GeV at 10 GeV and the cosmic-ray data of $2\sim3$ GeV covering a wide energy region. An effect of finite width of the mass distribution will be seen in the accelerator energy region near the threshold as was discussed in the preceding section. Here we will present the effect seen in a relation between prong number and average value of P_T, which is shown in Fig. 25.[16),27),29),31),32)] The average value of P_T is nearly constant and independent of the prong number. In more detail, one finds slight decrease of P_T at the large multiplicity region, and the decrease is more pronounced for cases of the small incident energy as will be inferred from the effect of the energy restriction. Qualitative feature of the effect can be better understood by comparison with the calculated curve from a simple phase space consideration applied to 8 GeV/c pion interaction.

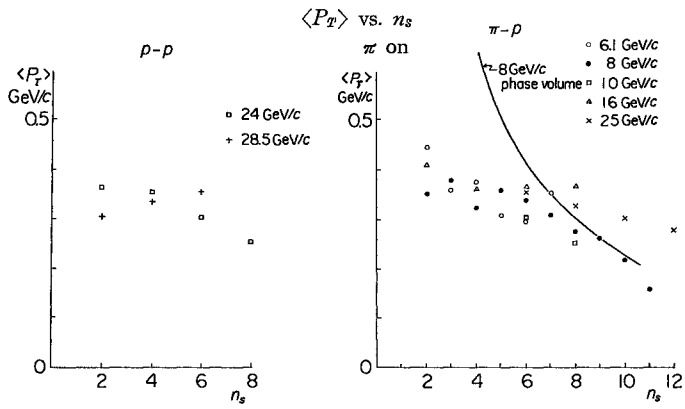

Fig. 25. The relation between n_s and $\langle P_T\rangle$ of secondary mesons from p-p interaction of 24 and 28.5 GeV/c and π^--p interaction of 6.1, 8, 10, 16 and 25 GeV/c. The curve is expected relation by the phase volume of 8 GeV incident pion.

The constancy of the Lorentz factor has to be discussed with considerations on the kinematical restriction. The experimental data show the constant Lorentz factor $\gamma_H^* \approx 1.4$ at energy of several ten GeV or more, while smaller values of γ_H^* are observed in the cases of lower incident energy. More in detail in the cases of incident energy around 10~20 GeV, one finds that γ_H^* is smaller as the multiplicity n_s increases in the events of the same incident energy. All of those features are explained as an effect of the kinematical restriction with the hypothesis of constant mass and constant Lorentz factor.

Finally we will discuss on comparison between the π-meson interaction and the proton interaction. We have already seen that the same hypothesis of constant mass and constant Lorentz factor consists with experimental data of both the interactions. Therefore, if their difference exists, it will be simply of the kinematical origin. This is just what the H-quantum theory concluded.

Acknowledgements

The authors are much indebted to the CERN P. S. group and emlusion group for providing us with the nuclear emulsion plates used in this experiment (Part I) to Professor Leprince-Ringuet of Ecole Poly-technique, France, to Professor C. M. G. Lattes of Instituto Central de Fisica, Universidade de Campinas, Brazil, and to Professor Y. Fujimoto of Department of Physics, Waseda University, Tokyo, for the kind arrangement of C.B.H. 81 films (Part II).

The authors are much indebted to Professor N. Ogita of Institute for Physical and Chemical Research for the kind arrangement of a computer OKITAC, valuable discussions and critical comments, to Professor Y. Fujimoto, and to Professor K. Yokoi of Department of Physics, Nagoya University, for valuable discussions and critical comments.

The authors express sincere thanks to Miss S. Hattori, Mr. K. Yamaguchi and Mr. H. Furihata of Department of Physics, Nagoya University, to Mr. Y. Isogane of Department of Physics, Kwansei Gakuin University, for scanning the plates, and to Mr. K. Nakano of Department of Physics, Waseda University, Tokyo, for his helps.

References

1) K. Niu, Nuovo Cim. **10** (1958), 994.
2) P. Ciok et al., Nuovo Cim. **8** (1958), 166.
3) G. Cocconi, Phys. Rev. **3** (1958), 1699.
4) S. Hasegawa, Prog. Theor. Phys. **26** (1961), 150; **29** (1963), 128.
5) Main contribution comes through the study of Bristol group, Chicago group, Poland group and ICEF project. See, for instance, E. Edwards, J. Losty, D. H. Perkins, K. Pinkau and J. Reynolds, Phil. Mag. **3** (1958), 237.
J. Duthie, C. Fisher, P. H. Fowler, A. Kaddours, D. H. Perkins and K. Pinkau, *Proceedings*

of the Moscow Cosmic Ray Conference, Vol. 135 (1960).
M. Schein, D. M. Haskin, E. Lohrman and M. W. Teucher, *Proceedings of the Moscow Cosmic Ray Conference*, Vol. 35 (1960).
A. G. Barkow, B. Chamney, D. M. Haskin, P. L. Jain, E. Lohrman, M. W. Jencher and M. Schein, Phys. Rev. **122** (1961), 2, 617.
P. Ciok, T. Coghen, J. Gierula R. Holynski, A. Jurak, M. Miesowicz, T. Saniewska, J. Pernergre and O. Stanisz, Nuovo Cim. **10** (1958), 741.
ICEF collaboration, Nuovo Cim. Suppl. 4 (1964), 1039, 1090.

6) S. Hasegawa and K. Yokoi, reported by S. Hayakawa, *Proceedings of the International Conference on High Energy Physics at CERN, 1962*, p. 643. See also S. Hayakawa, *Theoretical Physics, Lecture at 1963 Trieste Summer School* (I. A. E. A., Vienna, 1963), p. 485.
S. Hasegawa, Prog. Theor. Phys. **29** (1963), 128.

7) S. Sakata, Prog. Theor. Phys. **16** (1956), 686.

8) M. Taketani, private communication.

9) W. J. Fickinger, E. Pickup, D. K. Robinson and E. O. Salant, Phys. Rev. **125** (1961), 2082.
E. Pickup, D. K. Robinson and E. O. Salant, Phys. Rev. **125** (1961), 1386.

10) S. Hasegawa, H. Nanjo, T. Ogata, M. Sakata and K. Tanaka, Prog. Theor. Phys. **40** (1968), 673.

11) S. Hasegawa, H. Nanjo, T. Ogata, M. Sakata, K. Tanaka and N. Yajima, Prog. Theor. Phys. **41** (1969), 675.

12) For example: Y. Baudinet-Robinet, M. Morand, Tsai-Chu, C. Castagnoli, G. Dascola, S. Mora, A. Barbaro-Galtieri, G. Baroni and A. Manfredini, Nucl. Phys. **32** (1962), 452.
H. Meyer, M. W. Teucher and E. Lohrman, Nuovo Cim. **28** (1963), 1399.
B. Bhowmik and R. K. Shivpuri, Phys. Rev. **160** (1967), 1227.

13) M. H. Blue, J. J. Lord, J. G. Parks and C. H. Tsao, Phys. Rev. **125** (1961), 1386.

14) H. Winzeler, B. Klaiber, W. Koch, M. Nikolic and M. Schneeberger, Nuovo Cim. **17** (1960), **8.**
C. Bricman, M. Czejthey-Barth, J. P. Lagmaux and J. Sacton, Nuovo Cim. **20** (1961), 1017.
G. Cvijanowich, B. Dayton, P. Egli, B. Klaiber, W. Koch, M. Nicolic, R. Schneeberger, H. Winzeler, J. C. Gombe, W. M. Gibson, W. O. Lock, M. Schneeberger and G. Vanderhaeghe, Nuovo Cim. **20** (1961), 1012.
E. Lohrmann, M. W. Teucher and M. Schein, Phys. Rev. **122** (1961), 672.
A. A. Kamal and G. K. Rao, Nucl. Phys. **B2** (1967), 135.

15) V. V. Guseva, N. A. Dobrotin, N. G. Zelevinskaya, K. A. Katolnikov, A. M. Lebedev and S. A. Slavatinsky, *Proceedings of the International Conference on Cosmic Rays and Earth Storm, Kyoto, 1961;* J. Phys. Soc. Japan **17** Supple. A-III (1962), 375.

16) P. Dodd, M. Jobes, J. Kinson, B. Tallini, B. R. French, H. J. Sherman, I. O. Skillicon, W. T. Davis, M. Derrick and D. Radojicic, *Report of the Aix-en-Provence International Conference on Elementary Particles* (1961), p. 433.

17) N. Yajima and S. Hasegawa, Prog. Theor. Phys. **33** (1965), 184.

18) D. A. Galstyan, G. B. Zhdanov, M. I. Tretyakova, M. N. Shcherbakova and M. M. Chernarsky, Soviet Phys.-JETP **24** (1966), 280.

19) N. M. Duller and W. D. Walker, Phys. Rev. **93** (1954), 215.

20) K. Kobayakawa, K. Mori, K. Daiyasu and H. Yokomi, Nuovo Cim. **28** (1963), 992.

21) 100~400 GeV N. A. Dobrotin and S. A. Slavatinsky, *Proceedings of the International Conference on Cosmic Rays, Calgary, 1967.*

22) 1~10 TeV M. Schein, D. M. Haskin, E. Lohrman and M. W. Teucer, *Proceedings of the Moscow Cosmic Ray Conference*, vol. 35 (1960).

23) $\sum E_r$=3~20 TeV Japanese and Brazilian Emulsion Chamber Group, *Proceedings of the Conference on Cosmic Rays, Calgary, 1967.*

24) *p-p* 14 GeV/*c* M. Csejthry-Barth, Nuovo Cim. **32** (1964), 545.

25) *p-p* 19.8 GeV/*c* F. F. Abraham and R. M. Kalbach, Nuovo Cim. **26** (1962), 717.

26) p-p 23.5 GeV/c C. Cuijanowich, B. Dayton, P. Egli, B. Klaiber, W. Koch, M. Nikolic, R. Schneeberger, H. Winzeller, J.C. Combe, W.M. Gibson, W. O. Lock, M. Schneerberger and G. Vanderhaeghe, Nuovo Cim. **20** (1961), 1012.

27) p-p 28.5 GeV/c Reporter Talk by F. Turkot, CERN Report **1** (1968), 316.
Topical conference on high energy collisions of Hadron.

28) π^--p 6.1 GeV/c G. Bellini, M. di Corato, F. Duimio and E. Fiorini, Nuovo Cim. **40** (1965), 948.

29) π^+-p 8 GeV/c Raporter Talk by Czyzewski, CERN Report **1** (1968), 345.
Topical conference on high energy collisions of Hadron.

30) π^--p 16 GeV/c Raporter Talk by M. Miesovicz, *Proceedings of the International Conference on Cosmic Rays, Budapest, 1969*.

31) π^--p 16 GeV/c S.G. Goldstack, L. Riddiford, B. Tallini, B.R. French, W.W. Neal, J.R. Norbury, I.O. Skillicorn, W.T. Davies, J.H. Mulvey and D. Radojicic, Nuovo Cim. **23** (1962), 941.

32) π^--p 25 GeV/c J. W. Elbert, A. R. Erwin, S. Mikamo, D. Reeder, Y. Y. Chen, W.D. Walker and A. Weinberg, CERN Report Vol. 2 (1968), 244.
Topical conference on high energy collisions of Hadron.

33) π^--p 60 GeV/c Alma-Ata-Cracow-Dubna-Moscow, F.I.A.N. and Sofia-Ulan-Bator Collaboration, *Proceedings of the International Conference on Cosmic Rays, Budapest, 1969*.

34) π^--p 60 GeV/c B. Bogdon, I. Cincheza, J. Cohen, E.M. Friedländer, M. Maiduc, M. Marcu and T. Visky, *Proceedings of the International Conference on Cosmic Rays, Budapest, 1969*.

35) 100~1000 GeV V. V. Guseva, E. V. Penisov, N. A. Dobrotin, N. G. Zelevinskay, K. A. Kotelnikov, A. M. Lebedev, V. M. Maximenko, A. E. Morozov and S. A. Slavatinsky, Physics Series (Izvestia Academy Nauk U.S.S.R.) Vol. 33 (1969), p. 1408.